

# The Atmospheric Boundary Layer and the "Gray Zone" of Turbulence: A critical review

Rachel Honnert<sup>1\*</sup>, Georgios A. Efstathiou<sup>2</sup>, Robert J. Beare<sup>2</sup>, Junshi Ito<sup>3</sup>,  
Adrian Lock<sup>4</sup>, Roel Neggers<sup>5</sup>, Robert S. Plant<sup>6</sup>, Hyeyum Hailey Shin<sup>7</sup>,  
Lorenzo Tomassini<sup>4</sup>, Bowen Zhou<sup>8</sup>

<sup>1</sup>Météo-France, CNRM-CNRS UMR-3589, Toulouse, France

<sup>2</sup>Department of Mathematics, University of Exeter, Exeter, UK

<sup>3</sup>Department of Geophysics, Graduate School of Science, Tohoku University, Japan

<sup>4</sup>Met Office, Exeter, UK

<sup>5</sup>Institute for Geophysics and Meteorology, University of Cologne, Germany

<sup>6</sup>Department of Meteorology, University of Reading, Reading, UK

<sup>7</sup>National Center for Atmospheric Research, Boulder, Colorado, USA

<sup>8</sup>Key Laboratory for Mesoscale Severe Weather/MOE and School of Atmospheric Sciences, Nanjing University, Nanjing, China

## Key Points:

- The horizontal grid resolution of atmospheric models has become fine enough that models are able to partially resolve turbulent motions in the atmospheric boundary layer. This resolution regime comprises the "gray zone" of turbulence.
- The traditional parameterization methods for the representation of turbulence are no longer valid in the turbulence "gray zone".
- Due to the gray-zone problem, it is no longer the case that increases to the model resolution will necessarily improve the quality and usefulness of simulation results.
- We review the current efforts by modelers to overcome the gray-zone problems in order to provide useful simulations at high resolutions.
- We conclude that the task is far from being hopeless, and propose that extensions to the approaches being developed for this field may also prove valuable for other geophysical modeling problems.

---

\*CNRM UMR 3589, Météo-France

42, avenue Gaspard Coriolis  
31057 Toulouse cedex 01, FRANCE

Corresponding author: R. Honnert, [rachel.honnert@meteo.fr](mailto:rachel.honnert@meteo.fr)

**Abstract**

Recent increases in computing power mean that atmospheric models for numerical weather prediction are now able to operate at grid spacings of the order of a few hundred meters, comparable to the dominant turbulence length scales in the atmospheric boundary layer. As a result, models are starting to partially resolve the coherent overturning structures in the boundary layer. In this resolution regime, the so-called boundary-layer "gray zone", neither the techniques of high-resolution atmospheric modeling (a few tens of meters resolution) nor those of traditional meteorological models (a few kilometers resolution) are appropriate because fundamental assumptions behind the parameterizations are violated. Nonetheless, model simulations in this regime may remain highly useful. In this paper, a newly-formed gray-zone boundary-layer community lays the basis for parameterizing gray-zone turbulence, identifies the challenges in high-resolution atmospheric modeling and presents different gray-zone boundary-layer models. We discuss both the successful applications and the limitations of current parameterization approaches, and consider various issues in extending promising research approaches into use for numerical weather prediction. The ultimate goal of the research is the development of unified boundary-layer parameterizations valid across all scales.

**1 Introduction****1.1 Boundary-Layer Turbulence**

The atmospheric boundary layer (ABL) occupies the lowest part of the atmosphere, where most human activities take place and where weather phenomena have significant impacts on the anthropogenic and natural environment. The ABL is in direct contact with the surface and responds to surface forcings on a time scale of about an hour (Stull, 1988). In contrast to the free troposphere, which is located immediately above, the ABL is readily identified by its highly turbulent nature, which is driven by its constant interaction with the surface. Heat, moisture, momentum and contaminants are transferred and mixed by turbulent eddies having a variety of scales, ranging from a few meters to kilometers. Only under extremely stable conditions, when surface cooling is very strong and winds are very light, does turbulence cease in the ABL.

Turbulent eddies dominate the atmospheric micro-scales (cf. Orlanski, 1975). They are associated with various atmospheric phenomena such as strong gusts, pollutant dispersion, frost and fog that have significant social and economical impacts. The largest turbulent structures have scales on the order of the ABL height (about 1-3 km), while the smallest structures are dissipated at a few millimeters.

The convective ABL (CBL) commonly occurs during daytime over continental land, and is characterized by a surface that is warm compared to the air immediately above, resulting in strong surface heat fluxes. Such fluxes give rise to buoyant updraft motions, similar to warm Rayleigh-Bénard structures, called thermals, which are convective eddies extending from the surface to the top of CBL. They are associated with the peak of the energy containing scales shown in Fig. 1. The thermals are transitory structures that can move as they evolve. They break up to form smaller eddies so that their energy cascades from scale to scale through a continuous spectrum of eddy size called the "inertial sub-range" of turbulence until the Kolmogorov scale is reached and the energy is dissipated (cf. Fig. 1).

Supplementing the thermal production of turbulence, mechanical production of turbulence results from the wind shear in the ABL (e.g. due to the fact that wind "vanishes" at the surface), and this can also affect the structure and turbulent transfer in the ABL. Wind shear affects the boundary layer thermals, tilting them or weakening them. Under conditions when the wind is strong or the temperature flows are small (for example in the early morning), boundary layer thermals may be organized into convective rolls

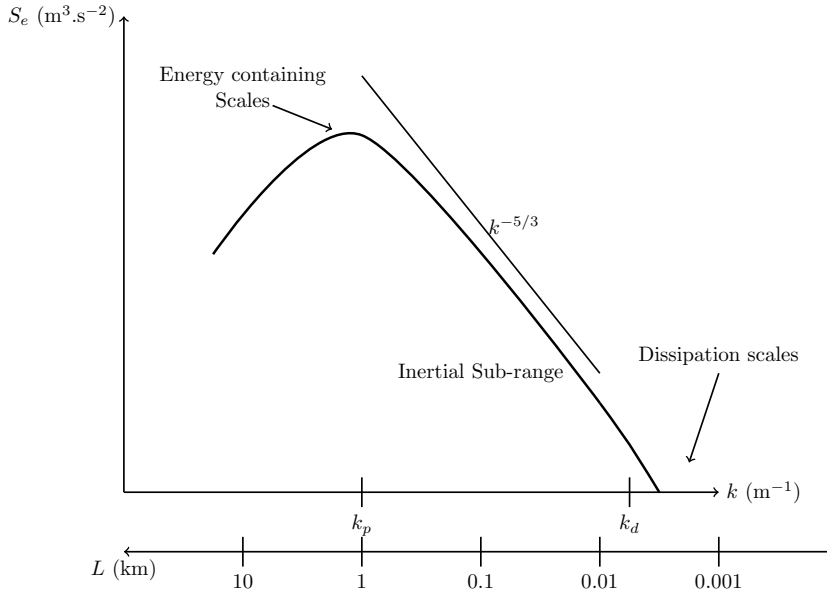


**Figure 1.** A schematic diagram of the turbulent kinetic energy in the CBL, plotted as a log-log graph as a function of scale. The spectral density of turbulent energy ( $S_e$ ) is shown as a function of wave number  $k$ , and of the corresponding length scale  $l = 2\pi/k$ .

78 or cloud streets, which are quasi-linear two-dimensional structures (Young et al., 2002).  
 79 However, under strong surface heating and light winds a regime of *free convection* oc-  
 80 curs in the CBL with thermals dominating the transfers of heat, momentum and mois-  
 81 ture from the surface to the overlying ABL and thence to the free troposphere.

82 The convection inside the CBL is often dry, with no latent heat release within the  
 83 updrafts. However, if the moisture content is sufficient then shallow clouds (cumulus or  
 84 stratocumulus) may appear at the top of the ABL where thermals reach their lifting con-  
 85 densation level. Deep moist convection refers to coherent turbulent motions of moist air  
 86 well into the troposphere and the development of associated deep clouds such as cumu-  
 87 lus congestus or cumulonimbus. Although shallow clouds at the top of the ABL will be  
 88 of interest here, we do not discuss deep clouds in any detail, excepting in so far as we  
 89 may be concerned with ensuring the appropriate interactions with initiating motions from  
 90 ABL turbulence.

## 91 1.2 Turbulence modeling and the Terra Incognita

92 Traditionally, global models of the atmosphere use grid lengths on the order of 10 km  
 93 or more, but limited-area mesoscale forecasting models may use grid lengths as low as  
 94 1 km. Thus, turbulent eddies are usually filtered out from meteorological models and  
 95 the impact of turbulent transfer on the larger scale flow is parameterized through the  
 96 use of boundary layer or turbulence schemes.

97 For modeling at relatively coarse grid lengths, which are larger than the scales of  
 98 the largest eddies, the turbulence is entirely sub-grid (or filtered). The corresponding  
 99 ABL parameterization schemes are designed to handle 1D vertical turbulent transfers  
 100 that arise from the effects of the full spectrum of unresolved turbulent eddies. An ad-  
 101 ditional shallow convection scheme may be needed to parameterize associated shallow  
 102 cumulus clouds (cf. Section 3.4).

103 Modeling at fine grid lengths of  $O(10\text{ m})$  occupies the regime of large-eddy sim-  
 104 ulation (LES), where models are able to resolve explicitly most of the turbulent motions.  
 105 More specifically, simulations may be considered to be LES when the grid length is sub-  
 106 stantially smaller than the dominant turbulence length scales (i.e.  $l_p = 2\pi/k_p$  in Fig. 1).  
 107 Sub-grid turbulence is considered to be isotropic when the grid scale lies within the in-  
 108 ertial sub-range (Fig. 1) and the dominant turbulence length scales become very well-  
 109 resolved on the numerical grid (see Sullivan and Patton (2011) for example). At these  
 110 resolutions sub-grid turbulent transfers are therefore 3D and the role of the sub-grid pa-  
 111 rameterization is to take account of the transfer of energy from the smallest resolved scale  
 112 to the dissipation scales ( $k_d$ ) across a clearly-defined inertial sub-range.

113 The advance of atmospheric modeling from its infancy in the 1950s to its widespread  
 114 operational use today has been strongly related to the increase of available computer power.  
 115 In particular, the development of high performance supercomputers has led to a signif-  
 116 icant increase of the horizontal grid resolution in numerical weather prediction. As res-  
 117 olution becomes finer, models start to resolve deep convective clouds. Weather centers  
 118 around the world are now using high-resolution regional models for weather prediction  
 119 or climate purposes. The UK Met Office runs its UK variable resolution model (UKV)  
 120 with a 1.5 km grid length over the British isles (Lean et al., 2008) while Météo-France  
 121 uses the AROME-France convective scale model at 1.3 km (Seity et al., 2011) alongside  
 122 an ensemble system at 2.5 km (Raynaud & Bouttier, 2017). In the convection-allowing  
 123 regime, deep convective structures become partially resolved and no longer occupy small  
 124 fractional areas of the grid. Therefore, the use of conventional deep convective param-  
 125 eterizations at these resolutions becomes highly questionable and they are often switched  
 126 off.

127 Pushing towards higher resolutions with grid lengths of  $O(100\text{ m})$ , atmospheric mod-  
 128 els become able to partially resolve the largest turbulent structures in the ABL, such as  
 129 the strong thermals in the CBL. Recent attempts to run such high-resolution atmospheric  
 130 models for weather prediction applications include the Météo-France 500 m grid-length  
 131 AROME-airport (Hagelin et al., 2014) run in 2014 for the Single European Sky Air Traf-  
 132 fic Research project and the UK Met Office 333 m "London model" (Boutle et al., 2015)  
 133 which was operational for the 2012 London Olympics. Environment-Canada simulated  
 134 the urban climate of Vancouver using a grid length of 250 m during the Vancouver 2010  
 135 Olympic and Paralympic Games (Leroy et al., 2011).

136 Wyngaard (2004) first identified that when the size of the largest turbulence struc-  
 137 tures in the ABL is comparable to the model grid spacing, the fundamental assumptions  
 138 behind conventional turbulence parameterizations are violated. He named this resolu-  
 139 tion regime the *Terra Incognita*, and the concept broadened to become the *gray zone* of  
 140 turbulence in the mesoscale modeling community, focusing on the convective boundary  
 141 layer. In the CBL gray zone, the turbulence kinetic energy (TKE) is only partially re-  
 142 solved, in contrast to the LES resolution regime where it is mostly resolved and in con-  
 143 trast to the mesoscale regime where it is fully parameterized.

144 This paper is organized as follows. Section 2 describes the different facets of the  
 145 gray zone of turbulence and the related modeling problems. In Section 3 we present the  
 146 possible solutions that have been proposed in the literature so far, followed by a discus-  
 147 sion in Section 4. Conclusions are provided in Section 5.

## 148 2 Characteristics and challenges of the gray zone of turbulence

### 149 2.1 Definition of the gray zone of turbulence

150 Wyngaard (2004) first studied the terra incognita using near-surface observational  
 151 data from the Horizontal Array Turbulence Study (HATS) program. The purpose of the  
 152 HATS field program was to study the interaction between two scales of turbulence (re-

153 solved/filtered and sub-grid/sub-filtered), with the ultimate goal being the improvement  
 154 of LES parameterizations. The experimental setting consisted of two horizontal cross-  
 155 wind lines of sonic anemometers at two different levels. The filter operation was a filter  
 156 in time, with Taylor’s frozen-turbulence hypothesis being applied to convert to an  
 157 equivalent spatial filter.

158 Wyngaard (2004) defined the ”terra incognita” at  $l \approx \Delta$ , where  $l$  represents the  
 159 dominant turbulence length scale and  $\Delta$  represents the filter length scale. When con-  
 160 sidered in terms of a numerical model, the filter length must be interpreted as an effective  
 161 resolution rather than the grid length directly (e.g. Ricard et al., 2013; Skamarock,  
 162 2004). The effective resolution depends on the internal diffusion of the model. For in-  
 163 stance, a very diffusive atmospheric model may fail to resolve ABL turbulence even at  
 164 hectometric grid size  $\Delta x$ , if its effective resolution  $\Delta$  exceeds  $l$ .

165 Inspired by the pioneering work of Wyngaard (2004), Honnert et al. (2011) stud-  
 166 ied the characteristics of the CBL gray zone by averaging (coarse-graining) LES data from  
 167 a number of well-documented case studies: the International H<sub>2</sub>O project (Couvreur et  
 168 al., 2005), the Wangara campaign (Clarke et al., 1971), the African Monsoon Multidis-  
 169 ciplinary Analysis field campaign (Redelsperger et al., 2006), the Barbados Oceanographic  
 170 and Meteorological EXperiment (P. Siebesma et al., 2004), and the ARMCu case (Brown  
 171 et al., 2002) (cf. Fig. 2). The use of HATS data constrained Wyngaard’s 2004 analyses  
 172 to the surface layer, but the use of LES allows the gray zone of turbulence to be stud-  
 173 ied at higher levels throughout the ABL. The disadvantage is that results may become  
 174 sensitive to the quality of the LES. Honnert et al. (2011) used LES data as a reference  
 175 to document the transition of TKE and turbulent fluxes from the LES regime through  
 176 the CBL gray zone and into the mesoscale regime. Coarse graining of the turbulent struc-  
 177 tures in the LES data produces smoother fields at hectometric scales in the CBL gray  
 178 zone until the turbulent variability becomes completely sub-grid scale at the mesoscale.

179 Figure 2 presents horizontal cross-sections of vertical velocity at 500 m altitude (in  
 180 the middle of the ABL) at different horizontal scales ranging from 62.5 m (the LES data)  
 181 up to 8 km. This example was produced by coarse graining an LES dataset based on the  
 182 International H<sub>2</sub>O observational campaign (Weckwerth et al., 2004) using the Méso-NH  
 183 model (Lac et al., 2018; Lafore et al., 1998). In this example, the transition between the  
 184 CBL gray zone and the mesoscale occurs at around the 2 km scale, at which some weak  
 185 turbulent structure can be seen. Honnert et al. (2011) demonstrate that the transition  
 186 depends on the quantity under consideration: turbulent structures in the water vapor  
 187 mixing ratio field occur on larger scales than those associated with the vertical veloc-  
 188 ity, in agreement with De Roode et al. (2004).

189 Honnert et al. (2011) considered the largest turbulence length scales  $l$  in the CBL  
 190 to be represented by the sum of the ABL height  $z_i$  and the depth of the shallow cloud  
 191 layer  $z_c$ . The basic idea is that the horizontal size of the largest structures is closely linked  
 192 to their vertical extent. According to this scaling, Honnert et al. (2011) found the CBL  
 193 gray zone to extend between filter scales of  $0.2(z_i + z_c)$  to  $2(z_i + z_c)$ .

194 A complementary perspective is provided by Beare (2014), who defines an effec-  
 195 tive length scale for numerical models which accounts for the modeled energy dissipa-  
 196 tion emerging from both the discretised advection and the sub-grid schemes. Specifically  
 197 the effective dissipation length scale  $l_{d,\text{eff}}$  is given by  $l_{d,\text{eff}} = 2\pi/k_{d,\text{eff}}$ , where:

$$198 \quad k_{d,\text{eff}}^2 = \frac{\int_{k_0}^{k_1} k^2 S_e(k) dk}{\int_{k_0}^{k_1} S_e(k) dk} \quad (1)$$

199  $k$  is the wave number and  $S_e$  is the TKE power spectrum. Beare (2014) considers a CBL  
 200 gray-zone simulation to be one in which there is no clear separation between the pro-  
 201 duction length scales and the model dissipation scale. In other words, there is no iner-  
 202 tial sub-range in the model: recall Fig. 1. A similarity relationship as a function of  $z_i/l_{d,\text{eff}}$

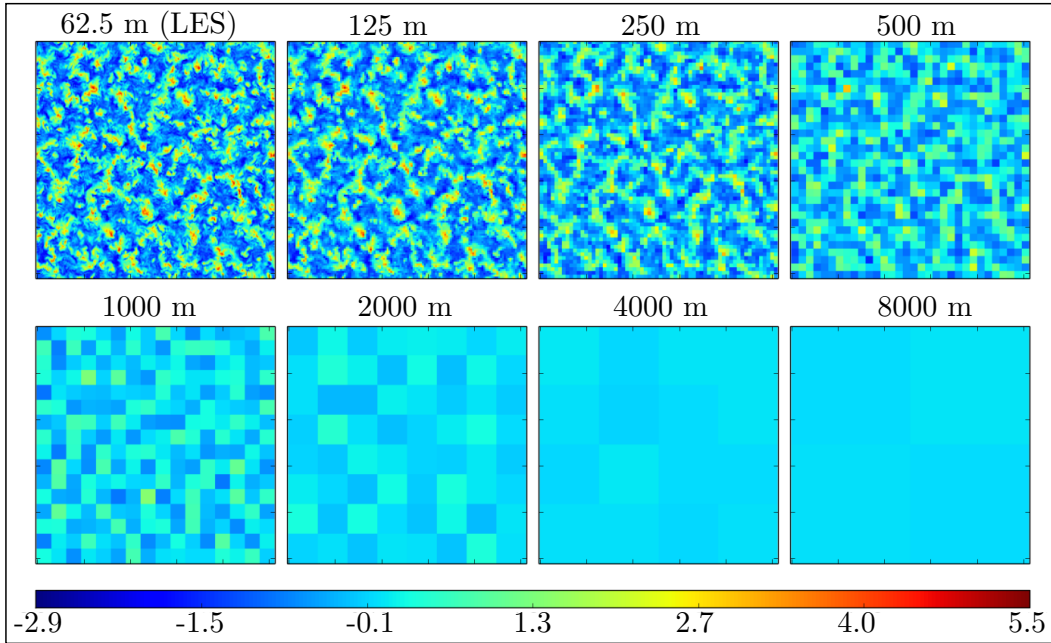


**Figure 2.** Horizontal cross-section of LES vertical velocity data at 500 m altitude (top left) and coarse graining of that data onto a range of scales up to 8 km. The units are  $\text{ms}^{-1}$ . Adapted from Honnert et al. (2011).

203 expresses the relative impact of the modeled dissipation scales on the physical produc-  
 204 tion and can be used as a definition for the CBL gray zone. Beare (2014) identifies the  
 205 transition between the CBL gray zone and the mesoscale regime as occurring at  $z_i/l_{d,\text{eff}} =$   
 206 0.7.

207 Figure 3 summarizes the different resolution regimes in atmospheric simulations  
 208 based on the above and other related studies. The CBL gray-zone transition is deter-  
 209 mined by the dissipation length scale analysis of Eq. 1 from Beare (2014), while the LES  
 210 transition is identified based on the findings of Sullivan and Patton (2011). Between the  
 211 mesoscale and LES limits, we identify both a *gray zone* and a *near gray zone* (see Ef-  
 212 stathiou et al., 2018). In the latter regime, most of the TKE is resolved ( $e_{\text{res}}/e_{\text{tot}} \gg 0.5$ )  
 213 but the simulations should not be considered as LES converging because the grid length  
 214 is not fine enough to present a clear inertial sub-range (see also Sullivan & Patton, 2011).  
 215 The regime might also be thought of as a coarse LES simulation and most practical ap-  
 216 plications treat the regime similarly to a standard LES. However, such a treatment can  
 217 have significant implications, especially in cases where the turbulence length scales are  
 218 evolving (Efstathiou et al., 2018). Taking  $l \approx z_i$  and  $z_i \approx 1000$  m, we find that LES  
 219 converging simulations can be achieved at  $\Delta x \sim 20$  m while the CBL gray zone is roughly  
 220 at  $2 \text{ km} > \Delta x > 200$  m.

## 221 2.2 Where is the 'truth'?

222 Turbulent motions are chaotic by definition. Turbulence modeling does not attempt  
 223 to describe them in full detail but introduces a statistical description of the turbulence.  
 224 Traditionally numerical weather prediction models simulate the Navier-Stokes equations  
 225 subject to an averaging or filtering operation. The mean quantities after filtering ( $\bar{f}$ ) are  
 226 often interpreted as representing the most probable state of the atmosphere assuming  
 227 that the distribution of possible sub-filter states is reasonably regular. Turbulence pa-

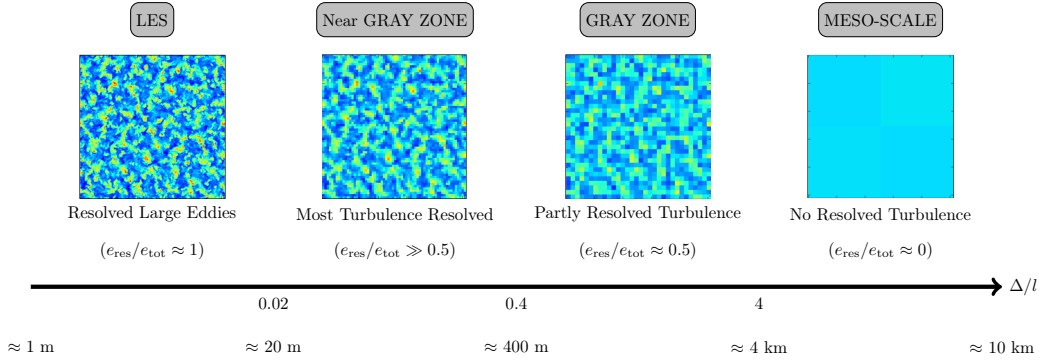


**Figure 3.** Schematic description of simulation regimes as a function of  $\Delta/l$ , where  $\Delta$  is the filter scale and  $l$  is the scale of the energy containing structures. Also shown is an estimate of typical model grid spacings. The horizontal cross-sections are taken from Fig. 2.

parameterizations for such models are often based on an ensemble average (Mellor & Yamada, 1982): i.e., an average over an infinite number of possible independent realizations of the flow. More generally, the averaging operator is assumed to fulfill Reynolds assumption (Stull, 1988, e.g.,  $\overline{gf} = \overline{g}\overline{f}$ , where  $f$  and  $g$  are functions and  $\overline{f}$  denotes the average of  $f$ ).

An alternative to ensemble averaging is to consider the filtering to be a time or space average. This approach is taken, for instance, when researchers average LES output data in order to characterize turbulent statistics (Covreux et al., 2010; A. P. Siebesma & Cuijpers, 1995, see also Sections 2.1 and 2.4) and to develop mesoscale parameterizations (e.g. Rio et al., 2010). If a spatial averaging scale is sufficiently large as to sample many eddies then there is often no practical difference between ensemble and spatial averaging. However, for a grid scale that is hectometric the form of the assumed averaging operator becomes crucial.

Using a space-time filter at scales of the gray zone of turbulence, model output fields should become turbulent, and partially-resolved turbulent structures appear (cf. Fig. 2). Such outputs represent one possible state of the atmosphere on the filtered scales. Real-scale experimental data represent only one possible state of the atmosphere also, and this would likely differ from the model state even if one were to have a perfect model.

### 2.3 Transition from sub-grid to resolved turbulence

As discussed above, turbulence in the CBL gray zone is partially resolved. Using LES data, the partitioning of turbulent energy into that which is sub-filter and that which is resolved can be computed for a given filter. The partition will depend upon the filter scale and the size of the turbulent structures. Honnert et al. (2011) considered such partitions for TKE and turbulent fluxes across the transition from the LES converging regime to the mesoscale limit in cases of free dry and cloudy CBLs. The partition function was scaled using the similarity parameter  $\Delta x/(z_i + z_c)$  with  $\Delta x$  being the coarse-graining filter scale. Figure 4 shows such a transition curve for the TKE. The approach has also been extended to other types of ABL (Shin & Hong, 2013).

The transition curve for the partitioning of turbulent quantities across scales has become widely used as a reference tool and a test-bed for the development and testing of parameterizations for the CBL gray zone (Boutle et al., 2014; Efstathiou & Beare, 2015; Ito et al., 2015; Malavelle et al., 2014; Shin & Hong, 2015; Shin & Dudhia, 2016).

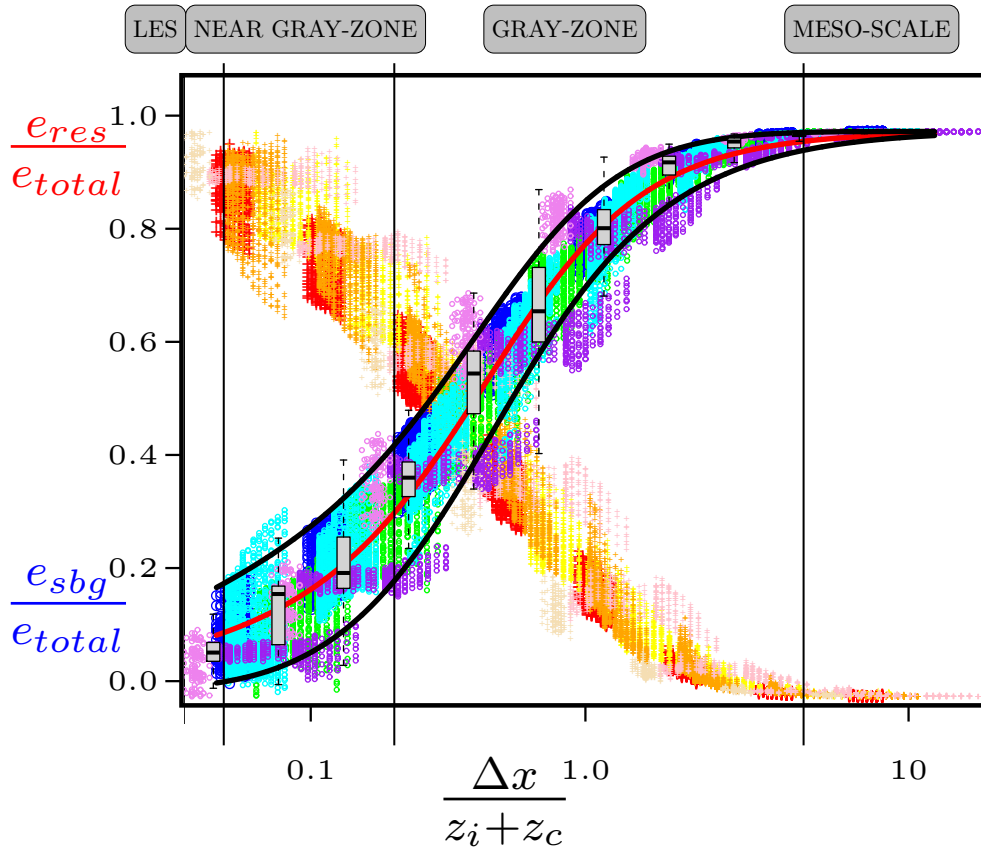


**Figure 4.** Functions showing the partition of the total TKE  $e_{total}$  into resolved ( $e_{res}$ ) and sub-grid ( $e_{sbg}$ ) parts, as a function of  $\Delta x/(z_i + z_c)$  (from Honnert et al., 2011):  $e_{res}/e_{total}$  is in warm colors and  $e_{sbg}/e_{total}$  is in cold colors. A similarity relation was found to hold in the CBL at altitudes  $z$  between  $0.05z_i$  and  $0.85z_i$ .

260 Honnert et al. (2011) evaluated the behavior of a state-of-the-art mesoscale model  
 261 (Méso-NH) in the CBL by comparing simulations at different scales against the refer-  
 262 ence curve of Fig. 4. Within the CBL gray zone, the resolved turbulence was found to  
 263 be too large when the model’s turbulence scheme was used without its mass-flux part.  
 264 The scheme did not mix the boundary layer efficiently enough, regardless of the mixing  
 265 length scale parameter that was used within the scheme to calculate the diffusivity. In  
 266 contrast, Honnert et al. (2011) found the resolved turbulence to be too weak when the  
 267 mass-flux scheme component of the scheme was activated. This effect strongly depends  
 268 on the mass-flux scheme (Shin & Dudhia, 2016). One of the mass-flux-type ABL schemes  
 269 tested in Shin and Dudhia (2016) showed a strong resolved turbulence even though the  
 270 mass-flux component was activated, because the mass-flux part was not large enough to  
 271 estimate the vertical transport by strong updrafts.



## 2.4 Traditional assumptions in models of the atmospheric boundary layer challenged by the gray zone of turbulence

The results discussed in Sect 2.3 illustrate that in the transition between sub-grid and resolved turbulence, traditional assumptions made in models of the atmospheric boundary layer, either at coarse or at very fine resolutions, are no longer valid in the gray zone of turbulence.

Large-scale models assume that the filter length scale (and also the related grid length of the model) is much larger than the important turbulent length scales in the boundary layer, and that therefore the representation of turbulence in the boundary layer does not strongly depend on the resolution of the model. They additionally assume, as mentioned in Section 2.2, that turbulent transfer is represented by an ensemble average of all possible flow realizations inside each grid box and as a result only the mean effects of turbulent motion are considered. On the opposite end of the spectrum, LES models require that the inertial sub-range is well resolved and so that the sub-grid turbulence scheme depends on model resolution in straightforward ways that can be deduced from scaling arguments. In neither case, however, is there any guarantee of an appropriate scale-awareness of the sub-grid turbulence within the gray zone of turbulence.

Another important issue is that large-scale models assume that sub-grid turbulent transport is dominated by the vertical component, and are therefore one-dimensional. However, neither is the sub-grid turbulence isotropic in three dimensions as commonly assumed by LES models. Thus, the gray zone of turbulence raises issues around the extent of anisotropy.

Wyngaard (2004) rigorously analyzed the turbulent momentum fluxes in the surface ABL with data from an anemometer array. The arrangement is illustrated in Fig. 5. He showed that some production terms for turbulent fluxes that may be negligible in the LES and mesoscale limits can nonetheless be significant in the gray zone of turbulence. Such terms are associated with anisotropy of the flow. It is important to bear in mind however, that the buoyancy-driven turbulence which dominates in the middle of the CBL is more strongly uni-directional than the shear-driven turbulence which plays an important role in the surface layer.

Honnert and Masson (2014) use LES coarse-graining of idealised CBL simulations to assess the scale dependence of turbulence production terms for TKE in the CBL above the surface layer. They show that 3D dynamical production terms become non-negligible over flat terrain at resolutions finer than  $0.5(z_i+z_c)$ , a result which implies that for such scales then 1D parameterizations do not provide an adequate representation of the TKE. According to Honnert and Masson (2014) the turbulence is anisotropic at about  $0.02 \leq \Delta x/(z_i+z_c) \leq 0.5$ . This range is consistent with the analysis of Beare (2014) for defining the CBL gray-zone onset from a different perspective (Section 2.1). Interestingly, Efstathiou and Beare (2015) also related the gray-zone onset to the need for different treatments of vertical and horizontal diffusion in their sub-grid model when simulating a quasi-steady state CBL.

Moreover, in both large-scale models as well as LES models, sub-grid turbulence schemes are usually assumed to be deterministic. Transport in the CBL is characterised by a population of turbulent eddies that cover a range of scales. With increasing model resolution the largest eddies are resolved first. Assuming that a space-time filtering approach is being taken, as in most traditional large-scale models of the ABL, then the part of the eddy size distribution that remains sub-grid will become increasingly under-sampled, with few of the largest unresolved eddies being present on the scale of a grid cell. Thus, one expects to find stochastic behavior near the grid scale in the gray zone of turbulence, and the traditional assumption that the number of eddies or updrafts in each grid cell

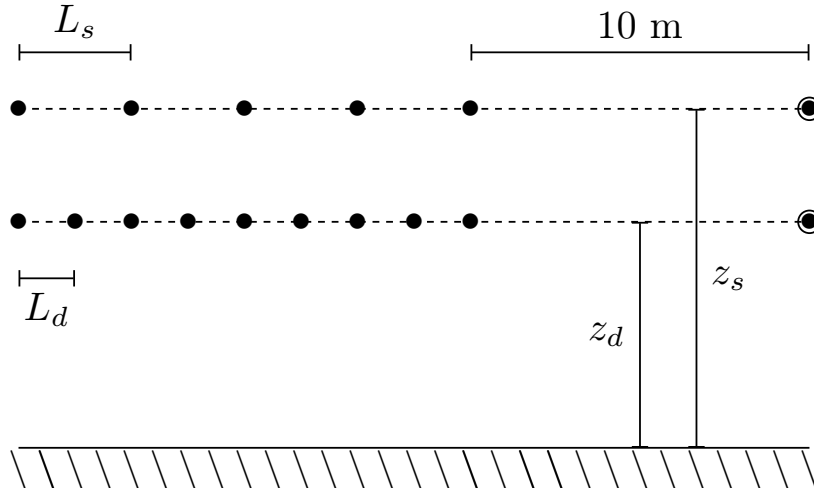


**Figure 5.** Arrangement of sonic anemometers in the HATS experiments. Single and double arrays are located at heights  $z_s$  and  $z_d$  above the surface, and the crosswind separation between individual sonic anemometers at each height is  $L_s$  and  $L_d$  respectively. Two reference sonic anemometers (circled) are used to monitor the possibility of flow interference among the anemometers in the  $s$  and  $d$  arrays. Adapted from Sullivan et al. (2003)

322 is large enough to fulfill the "law of large numbers" underlying deterministic parame-  
 323 terizations is no longer valid.

324 Other important assumptions concern the representation of non-local expressions  
 325 in turbulence parameterizations. These are often formulated using mass flux approaches  
 326 (Section 3.4). As resolution increases, the large non-local motions will be partially re-  
 327 solved within the CBL gray zone. Mass-flux schemes used in meso-scale models assume  
 328 that the non-local part of the flux is attributable to these CBL thermals, that the re-  
 329 sulting flux is stationary and that the thermals occupy a relatively small area compared  
 330 to their more quiescent environment. Each model grid cell is supposed to contain both  
 331 a meaningful number of such thermals and their associated compensatory subsidence.  
 332 The assumption that the vertical velocity in the grid cell is zero or that the thermal frac-  
 333 tion is negligible breaks down by definition in the CBL gray zone where the thermal length  
 334 scale is on the order of the grid spacing.

## 335 2.5 Gray zone in an evolving convective boundary layer

336 Atmospheric models have a fixed grid length but the turbulence characteristics may  
 337 change in the course of a simulation. A pertinent example is the development of a CBL  
 338 that is strongly forced by surface heating, as often occurs over cloud-free land during the  
 339 morning. Figure 6 shows the evolution of such a developing CBL in a case study using  
 340 the Met Office Large Eddy Model (LEM) with  $\Delta x = 200, 400$  and  $800$  m (Efstathiou  
 341 et al., 2016). Shaded in gray are the times and heights where the flow is considered to  
 342 be in the CBL gray zone, according to the analysis of Beare (2014). In the  $800$  m run  
 343 the CBL remains in the gray zone throughout the simulation. In contrast, the  $200$  and  
 344  $400$  m simulations lie in the CBL gray zone only during the early CBL development, al-  
 345 beit with the  $400$  m run taking somewhat longer to transition to the coarse LES regime.  
 346 Moreover, near the surface and the top of the ABL the CBL gray zone persists for longer  
 347 since the turbulent length scales are affected by the presence of these boundaries to the  
 348 turbulent part of the flow. Thus, we see that a simulated evolving CBL can be in dif-

349 ferent resolution regimes that can vary both in time and space depending on the scale  
 350 of the convective structures.

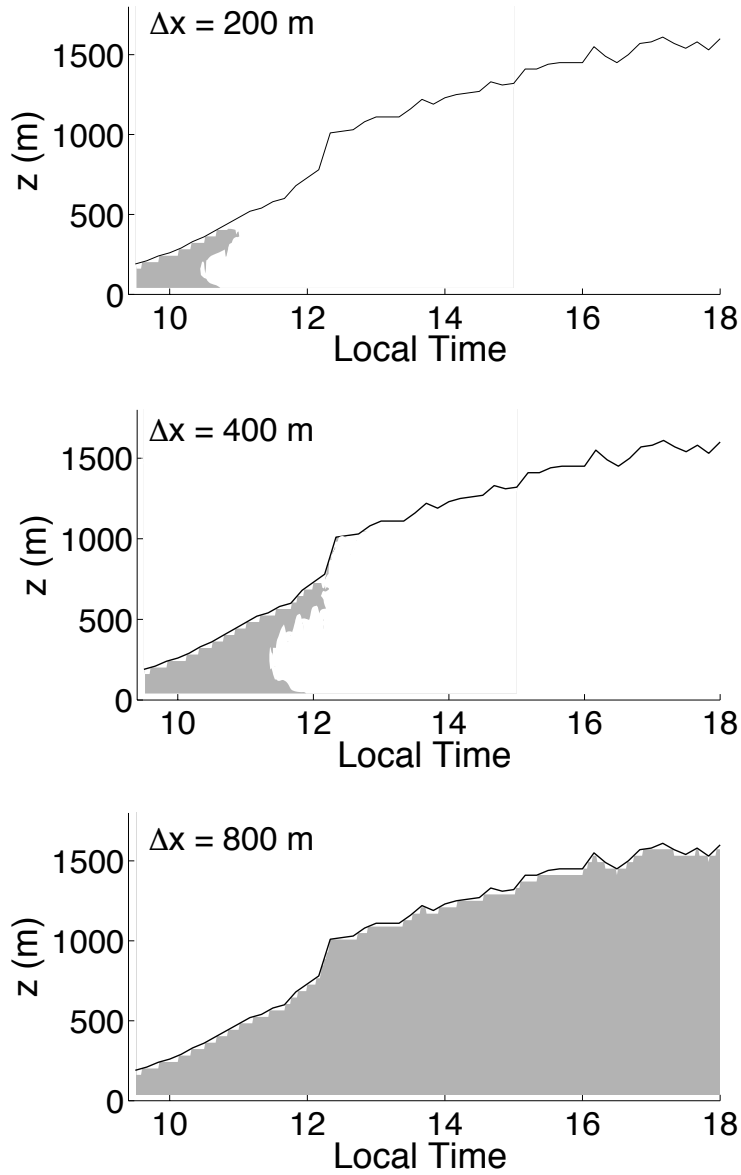


**Figure 6.** The time evolution of the CBL depth (black line) in a case study simulation of an evolving CBL (Efstathiou et al., 2016) using three different horizontal grid spacings. Shaded in gray color are the parts of the CBL that are considered to be in the gray zone of turbulence according to the analysis of Beare (2014).

351 A particular problem in gray-zone simulations of an evolving CBL concerns the spin-  
 352 up of realistic levels of resolved TKE from the initial state. Efstathiou et al. (2016); Zhou

et al. (2014) and Kealy et al. (2019) have shown that spin-up is significantly delayed with coarsening resolution within the CBL gray zone. Shin and Hong (2015) also pointed out that their gray-zone CBL parameterization delayed the spin-up of resolved motions. The consequence of delayed spin-up is that temperature profiles can become super-adiabatic in response to the lack of non-local mixing that the resolved TKE would otherwise provide. Such a delay can also have significant implications when simulating the full diurnal cycle of convection, including the transition from shallow to deep moist convection (e.g. Petch et al., 2002).

## 2.6 From shallow to deep moist convection to synoptic-scale systems

Various properties of convective clouds and mesoscale systems in sub-kilometric models have been demonstrated to be rather sensitive to the choices made in the formulation of turbulent mixing within the gray zone of turbulence. Some good examples can be seen in the idealized modeling studies of Bryan and Morrison (2012); Craig and Dornbrack (2008); Fiori et al. (2010); Verrelle et al. (2015). Similar case studies in realistic conditions can be found in Bengtsson et al. (2012); Duffourg et al. (2016); Martinet et al. (2017); Ricard et al. (2013), while a rich statistical perspective is provided by Stein et al. (2015). The studies of Tomassini et al. (2016); Sakradzija et al. (2016) focus particularly on the interplay between boundary-layer turbulence and shallow convective clouds.

The representation of boundary-layer turbulence in numerical weather prediction models does not only interact with (shallow and deep) convective cloud, but is also closely interrelated with the representation of the land surface, the atmospheric dynamics, and microphysics (Field et al., 2017). Boundary-layer processes are important even for synoptic scale weather systems. In the mid-latitudes, boundary-layer friction provides a damping mechanism for barotropic vortices through Ekman pumping (Boutle et al., 2015). Baroclinic developments are also dampened by changes to low-level stability which can be understood in terms of tendencies of potential vorticity that are produced by turbulent mixing processes (Adamson et al., 2006; Stoelinga, 1996). By contrast, in the tropics, boundary-layer dynamics may often act to enhance synoptic-scale systems. This is well illustrated by African easterly waves, for which potential vorticity generation by boundary-layer processes can feed into the dynamics and contribute to wave growth (Tomassini et al., 2017). Moreover, boundary-layer turbulence is important in the establishment of summer time low-level jets over land which may transport high moist static energy air and feed deep convective development (Chen & Tomassini, 2015). This mechanism is particularly relevant in monsoon regions and at continental-scale precipitation margins.

## 3 Modeling the atmospheric boundary layer in the gray zone of turbulence

As explained in Section 2, the gray zone of turbulence is not a physical phenomenon, but rather it describes interrelated problems that arise due to the assumptions behind our current turbulence and shallow convection schemes. In this section, we consider some possible solutions that have been proposed to those problems, and their limits.

### 3.1 Full transport model approach

Wyngaard (2004) suggested using the full transport equations for representing the sub-grid scalar transport of a conserved scalar field  $c$  at gray-zone resolutions in the boundary layer. Without imposing the usual assumptions in mesoscale modeling he introduced a tensor form for the parameterization of the turbulent flux ( $f_i$ ) of  $c$  (see Appendix A for an outline of the derivation):

$$f_i = -K_{ij} \frac{\partial \bar{c}}{\partial x_j} \quad (2)$$

where  $K_{ij}$  is a tensor form of the eddy diffusivity which is a function of a turbulent time scale, the shear tensor and the Reynolds stress. Thus, Wyngaard’s 2004 model can be viewed as a generalized form of the usual diffusion approach which can account for anisotropy of the turbulence. As implied by the arguments of Section 2.4, this extension is an attractive possibility for modeling sub-grid fluxes from the LES to the mesoscale limit. The eddy diffusivity is a function of the flow and should be treated as a tensor and not as a scalar. Other elements of the full tensor may become important in the gray zone of turbulence (such as the tilting terms) since the heterogeneity of the convective structures might impose strong horizontal gradients.

Hatlee and Wyngaard (2007) first implemented the approach to study HATS data close to the surface. Kelly et al. (2009) extended the approach to the ocean surface layer by analyzing data from the OHATS (Ocean Horizontal Array Turbulence Study) observations and developed a simple parameterization for pressure fluctuation induced by moving surface waves. The full transport equations have been implemented by Ramachandran and Wyngaard (2011) and Ramachandran et al. (2013) in simulations of a convective case in the ocean. They showed that the anisotropic terms in the sub-filter flux equations can indeed become important when the grid length approaches the dominant production scales, in accordance with the HATS analyses of Hatlee and Wyngaard (2007). Therefore their model produced much better estimations of the momentum and heat fluxes compared to the standard eddy-diffusivity approach.

The full transport model appears to be a promising first approach to modeling in the gray zone of turbulence. Such an approach is expected to behave analogously to a higher-order closure scheme in the mesoscale limit with the appropriate choice of length scales (Wyngaard, 2004). However, the shortage of validation studies, and in particular the absence of a full implementation of the method across the complete range of modelling scales, does not allow firm conclusions to be drawn on the performance or the practical applicability of the scheme.

### 3.2 TKE turbulence modeling

TKE-based turbulence models determine eddy diffusivities based on the magnitude of sub-grid TKE,  $e$ , specifically:

$$K_c = C_c l_m \sqrt{e} \quad (3)$$

where  $C_c$  is a constant which may depend on the variable  $c$  of interest, while  $l_m$  is the mixing length.  $l_m$  may be set using the CBL height in mesoscale models, but is based on the grid spacing in LES applications of the approach. The sub-grid TKE itself is obtained by solving its prognostic equation:

$$\frac{\partial \bar{e}}{\partial t} = - \left( \overline{u_i} \frac{\partial \bar{e}}{\partial x_i} + \frac{\partial \overline{u'_i e}}{\partial x_i} + \frac{1}{\rho_0} \overline{u'_i} \frac{\partial \overline{p'}}{\partial x_i} - \nu \frac{\partial^2 \bar{e}}{\partial x_i^2} \right) - \overline{u'_i u'_j} \frac{\partial \overline{u'_j}}{\partial x_i} + \beta \overline{u'_3 \theta'} - 2\nu \left( \frac{\partial \overline{u'_j}}{\partial x_i} \right)^2 \quad (4)$$

where  $\theta$  is the potential temperature,  $p$  is the pressure,  $\nu$  is the molecular diffusivity and  $\beta$  is the buoyancy parameter. Other symbols have been already introduced. The first (in parentheses) term on the right hand side describes the tendency of  $e$  due to large scale advection, turbulence, pressure gradient correlations and molecular diffusion, the second and third terms represent the production of turbulence by wind shear and buoyancy respectively and the last right-hand side term is the dissipation of  $e$ .

#### 3.2.1 Pragmatic approaches over complex terrain

Turbulence parameterizations for atmospheric models have been developed based on assumptions that are, strictly speaking, only valid for horizontally homogeneous and flat terrain, and may not be suitable for complex terrain. For example, Monin-Obukhov similarity theory is commonly used to compute surface fluxes and assumes horizontally

447 homogeneous fluxes from the surface into the boundary layer. In complex terrain, Arnold  
 448 et al. (2012) recommends as a first approach the use of fully prognostic three-dimensional  
 449 TKE schemes for grid spacings between 100 and 300 m.

450 Beljaars et al. (2004) proposed a parameterization of turbulent orographic form drag  
 451 that takes into account the model resolution and is used at ECMWF. However, while  
 452 there are studies of the behavior of orographic drag in the gray zone of deep convection  
 453 (5 km resolution), (Sandu, ECMWF Newsletter 150) there are none as yet at the hec-  
 454 tometric scales. At hectometric scales, it is not well understood which part of the drag  
 455 should be taken into account through an explicit parameterization of orographic drag  
 456 and which part by the turbulence scheme. We note that the model of the Met Office does  
 457 not include an orographic drag contribution at such scales. Moreover, the theoretical back-  
 458 ground of the processes involved is not well understood even at mesoscales (see Sandu,  
 459 ECMWF Newsletter 150). Hence, analysis of the problems in representing orographic  
 460 drag in the gray zone of turbulence is more difficult than an analysis based on the dy-  
 461 namic production of TKE in the turbulence scheme.

462 Over complex terrain in the CBL gray zone, the full three-dimensional effects have  
 463 been found to be important in the shear production term for TKE (Arnold et al., 2014;  
 464 Goger et al., 2018). Goger et al. (2018) therefore propose an extension of the 1D prog-  
 465 nostic TKE equation used in the COSMO (COntortium for Small-Scale Modeling) model  
 466 turbulence scheme because that scheme otherwise underestimates the TKE. The 1D form  
 467 considers only the contributions to shear production from vertical gradients of horizon-  
 468 tal winds, but Goger et al. (2018) supplement this with a further contribution of

$$469 \quad \left. \frac{\partial \bar{\epsilon}}{\partial t} \right|_{\text{shear}} = (C_s \Delta x)^2 \left[ \left( \frac{\partial \bar{u}}{\partial x} \right)^2 + \left( \frac{\partial \bar{v}}{\partial y} \right)^2 + \frac{1}{2} \left( \frac{\partial \bar{u}}{\partial y} + \frac{\partial \bar{v}}{\partial x} \right)^2 \right]^{\frac{3}{2}} \quad (5)$$

470 where  $C_s$  is chosen to be the Smagorinsky constant (see Section 3.3). This extension was  
 471 tested in simulations over the Alps for a grid length of 1.1 km and had beneficial effects.  
 472 The verification indicated improvement in the TKE on the slopes, which suggests that  
 473 the addition of 3D effects is particularly suitable for inclined surfaces.

### 474 **3.2.2 Adaptive length scales**

475 In order to incorporate scale-awareness (Section 2.4), various authors have attempted  
 476 to develop approaches for the gray-zone of turbulence that are based on rethinking the  
 477 mixing length that is used in TKE-based approaches (Eq. 3) or other semi-empirical length  
 478 scales used in higher-order turbulence models. Ito et al. (2015) for example, has proposed  
 479 an extension of Mellor-Yamada-Nakanishi-Niino (MYNN) model for the gray zone of tur-  
 480 bulence. The MYNN model is a higher-order turbulence closure designed for 1D mesoscale  
 481 applications (Nakanishi & Nino, 2009). The sub-grid TKE is predicted using an empir-  
 482 ical length scale to parameterize various terms. In the extension the length scale is mod-  
 483 ified in order to hold the TKE dissipation invariant to the grid resolution. To partition  
 484 the TKE into appropriate resolved and sub-grid contributions the extension also con-  
 485 sideres the partition function proposed by Honnert et al. (2011) (as discussed in Section 2.3).  
 486 Horizontal diffusion based on Ito et al. (2014) is also included in order to take account  
 487 of anisotropy (Section 2.4). Ito et al. (2015) showed that a CBL gray-zone simulation  
 488 employing this extension was able to realize reasonable vertical transports.

489 Kitamura (2015) used a coarse-graining approach on LES data from a CBL sim-  
 490 ulation in order to estimate the length scale dependence on grid spacing, assuming the  
 491 form of a TKE-based Deardorff (1980) model for the turbulent fluxes. Notably the es-  
 492 timated length scale was found to depend upon both the horizontal and vertical grid spac-  
 493 ings. Kitamura (2016) implemented the resulting mixing length formulations in a mod-  
 494 ified Deardorff (1980) model, which improved the representation of the vertical heat flux  
 495 and the magnitude of the resolved convection in the CBL gray zone.

496 Zhang et al. (2018) blended between the sub-grid turbulent mixing length scales  
 497 that are appropriate for the LES and mesoscale limits to create a grid-scale-dependent  
 498 3D TKE scheme. The scheme includes a non-local component in the vertical buoyancy  
 499 which is also down-weighted by a blending function (cf. Boutle et al., 2014) depending  
 500 on the resolution regime. The blended approach was implemented in WRF and exhib-  
 501 ited improved behaviour in comparison with a conventional TKE scheme.

Kurowski and Teixeira (2018) also proposed to pragmatically merge the mixing lengths  
 from LES and NWP formulations to obtain a mixing length for intermediate scales:

$$\left(\frac{1}{l_{BL}}\right)^2 = \left(\frac{1}{l_{1D}}\right)^2 + \left(\frac{1}{l_{3D}}\right)^2 + \left(\frac{1}{l_s}\right)^2 \quad (6)$$

502 where  $l_{3D}$  is Deardorff LES mixing length (Deardorff, 1980),  $l_s$  is a surface mixing length  
 503 (see Kurowski & Teixeira, 2018) and  $l_{1D}$  is the large scale NWP mixing length from Teixeira  
 504 and Cheinet (2004). In their formulation, the mixing length is smaller than the small-  
 505 est of the three components. Their merged mixing length does not explicitly depend on  
 506 resolution, but in practice it increases with increasing grid size until the mesoscales.

### 507 **3.2.3 Two turbulence kinetic energies**

508 A related approach has been proposed by Bhattacharya and Stevens (2016) who  
 509 introduce two turbulent kinetic energies in order to distinguish between the energy con-  
 510 tained in large eddies spanning the CBL and that within eddies that are sub-grid with  
 511 respect to the vertical grid spacing. The two energies are conceptually linked via the tur-  
 512 bulent energy cascade. Bhattacharya and Stevens (2016) formulated distinct length scales  
 513 to describe mixing and dissipation associated with each energy. However, the problem  
 514 remains of how to divide the energy due to the boundary-layer-scale eddies into resolved  
 515 and unresolved parts. The approach is yet to be tested in a weather or climate model.

### 516 **3.3 Extending the Smagorinsky-Lilly scheme into the gray zone of tur- 517 bulence**

The Smagorinsky-Lilly (Lilly, 1967; Smagorinsky, 1967) scheme is a widely-used  
 standard for large-eddy simulations of many and various engineering and geophysical flows.  
 Scalar fluxes are represented by:

$$f_i = -K_c \frac{\partial \bar{c}}{\partial x_i}, \quad (7)$$

as described in Appendix Appendix A (Eq. A3). The eddy diffusivity is expressed as

$$K_c = l_t^2 |\bar{S}| / \text{Pr} \quad (8)$$

518 where Pr is known as the Prandtl number,  $|\bar{S}|$  is the modulus of the shear tensor  $\bar{S}_{ij} =$   
 519  $(\partial \bar{u}_i / \partial x_j) + (\partial \bar{u}_j / \partial x_i)$ , and  $l_t$  is the turbulence mixing length. The specification is com-  
 520 pleted by choosing the mixing length to be  $l_t = C_s \Delta$  where  $C_s$  is known as the Smagorin-  
 521 sky constant. Following the analysis of Lilly (1967) it is often set to 0.17 although dif-  
 522 ferent values up to 0.23 have been suggested and used in atmospheric models. The Smagorin-  
 523 sky scheme acts in all three directions with the same eddy diffusivity. Comparing to Eq. 2,  
 524 the scheme is an approximate form of the full turbulent stress tensor model, valid when  
 525 the full turbulent stress tensor is assumed isotropic, such that  $K_{ij} = K_c \delta_{ij}$ .

#### 526 **3.3.1 Bounding approach**

527 Efstathiou and Beare (2015) showed that the standard Smagorinsky scheme be-  
 528 comes too diffusive in the CBL gray zone. Therefore, in order to reduce the over-damping  
 529 effect arising from the increase in mixing length  $l_t$  with horizontal resolution  $\Delta x$ , a mod-  
 530 ification was made in an attempt to conserve the effective diffusivity of the flow across  
 531

531 different grid lengths. As a first approximation, the vertical Smagorinsky diffusivity pro-  
 532 file was bounded so that values could not exceed those produced by a 1D mesoscale ap-  
 533 proach. The horizontal diffusion was handled by a 2D closure and allowed to vary in or-  
 534 der to account for anisotropy of the flow at CBL gray-zone resolutions. This bounding  
 535 approach was able to match the energetics of the coarse-grained fields across the tran-  
 536 sition from the LES to the mesoscale regime in a quasi-steady state CBL.

### 537 3.3.2 Dynamic Smagorinsky

538 The standard Smagorinsky approach is designed for the LES regime and assumes  
 539 a clear scale separation with the presence of a clear inertial sub-range (Section 2.4). The  
 540 idea behind a dynamic model is to treat  $C_s$  as a flow-dependent variable, which can be  
 541 estimated by comparing the resolved flow against the same flow filtered onto a coarser  
 542 “test” scale. The idea can also be extended through comparison of the resolved flow against  
 543 that at two different filtered scales in order to estimate a flow-dependent and scale-dependent  
 544  $C_s$ . The aim of such a scale-dependent dynamic model is to respect the characteristics  
 545 of the turbulence spectrum without necessarily requiring the resolved flow to lie within  
 546 the inertial sub-range. Hence, it is a promising extension of Smagorinsky that is well suited  
 547 to coarse LES resolutions (e.g. Kleissl et al., 2006; Mirocha et al., 2013) and perhaps even  
 548 to CBL gray-zone resolutions.

549 Efstathiou et al. (2018) modified and implemented a scale-dependent, Lagrangian-  
 550 averaged dynamic Smagorinsky sub-grid scheme based on Bou-Zeid et al. (2005) into the  
 551 Met Office Large Eddy Model. Extending an earlier study by Basu et al. (2008), they  
 552 found the approach to perform well for an evolving CBL in capturing the resolved tur-  
 553 bulence profiles in comparison with coarse-grained LES fields, especially in the *near gray-*  
 554 *zone* regime (Fig. 3). However, such a dynamic approach reaches a limit of applicabil-  
 555 ity if the test filter is required to sample the flow at a scale for which the turbulence is  
 556 not adequately represented by the model.

557 One way around this issue could be the use of the Dynamic Reconstruction Model  
 558 of Chow et al. (2005) which attempts to reconstruct the smallest resolved scales and uses  
 559 those to dynamically derive the sub-grid mixing length. Simon et al. (2019) tested this  
 560 approach to simulate a quasi-steady CBL at gray-zone resolutions and found significant  
 561 improvement over conventional schemes and especially compared to the standard Smagorin-  
 562 sky scheme.

## 563 3.4 Modifying boundary layer 1D non-local parameterizations

564 CBL thermals (cf. Section 2.4) are manifestations of non-local turbulence, and are  
 565 responsible for the development of a zone of counter-gradient fluxes at the top of the CBL  
 566 which is ill-represented by an eddy diffusivity form (Eq. 3).

567 In mesoscale models, the turbulent transport from the surface to the top of the ABL  
 568 by convective thermals can be parameterized by the use of an additional counter-gradient  
 569 term (Deardorff, 1972) so that,

$$570 \quad f_c = -K_c \left( \frac{\partial \bar{c}}{\partial z} - \gamma \right) \quad (9)$$

571 where  $f_c$  is the turbulent flux of  $c$  and  $\gamma$  is the counter-gradient term. More complex pa-  
 572 rameterizations have been based on the transient matrix (Stull, 1984)) or the mass-flux  
 573 scheme (Cheinet, 2003; Hourdin et al., 2002; Pergaud et al., 2009; Rio et al., 2010; A. P. Siebesma  
 574 et al., 2007; Tan et al., 2018). In a mass-flux scheme the turbulent flux is expressed as

$$575 \quad f_c = -K_c \frac{\partial \bar{c}}{\partial z} + M_u (c_u - \bar{c}) \quad (10)$$



576 where  $M_u$  is the mass-flux associated with the ABL thermals, and  $c_u$  is the mean value  
 577 of  $c$  inside the thermals. The second term on the right-hand side represents the trans-  
 578 ports by coherent thermal plumes whereas the first term is expressed in eddy diffusiv-  
 579 ity form and represents the contributions from smaller-scale more-localized eddies (Fig. 7).  
 580 This mass flux approach also lends itself naturally to extensions that treat shallow boundary-  
 581 layer clouds.

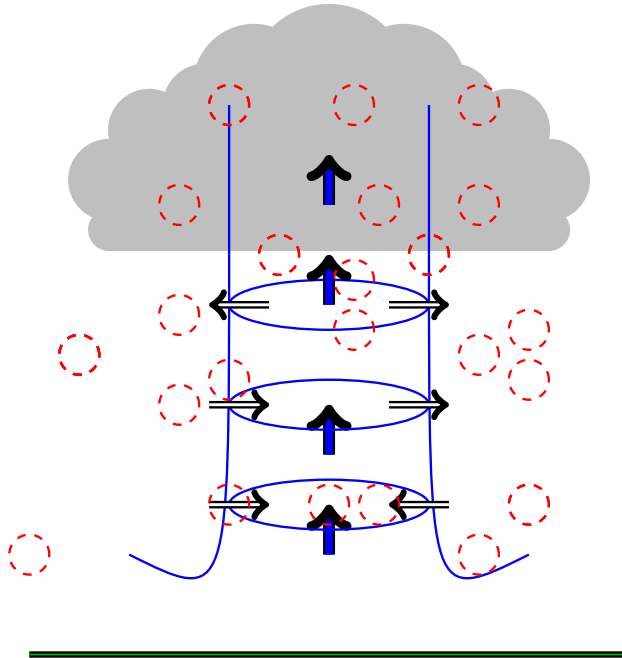


**Figure 7.** Schematic diagram of small local eddies (red dashed circles), contrasted against a non-local thermal (blue tube) which extends from the surface (green) to the cloud layer (in gray).

582 Representations of the form of Eqs. 9 and 10 are designed for mesoscale models but  
 583 the split provides an interesting starting point for possible gray zone treatments of tur-  
 584 bulance. As resolution increases the large non-local motions will be partially resolved within  
 585 the CBL gray zone for  $\Delta \sim z_i$  but the small eddies might remain purely sub-grid. With  
 586 this point in mind, the adaptation of mesoscale models to the CBL gray zone could be  
 587 achieved by revisiting traditional non-local ABL schemes.

588 A mass-flux scheme used at the mesoscales assumes that a non-local flux is created  
 589 by the CBL thermals. This flux is assumed to be stationary and is created by several  
 590 thermals which occupy small areas compared to their more quiescent environment. Each  
 591 model grid cell is supposed to contain both a meaningful number of updrafts and their  
 592 associated compensatory subsidence. Such assumptions break down by definition in the  
 593 CBL gray zone where the thermal length scale  $l$  is of the order of the grid spacing  $\Delta x$   
 594 (Section 2.4). Related issues have been studied in the context of the mass-flux represen-  
 595 tation of deep convective clouds and are discussed by Arakawa et al. (2011); Arakawa  
 596 and Wu (2013) for example.

597 Honnert et al. (2016) modified a mass-flux scheme for the CBL gray zone (Pergaud  
 598 et al., 2009), by generalizing the mass flux equations without the need for assumptions  
 599 that the vertical velocity in the grid cell is zero or that the thermal fraction is negli-  
 600 gible. In this framework, the velocity of the parameterized updraft is reduced when the  
 601 resolution increases, which then permits the model dynamics to produce resolved struc-

602 tures. The study also incorporates a dependency on the normalized resolution  $\Delta x/(z_i +$   
 603  $z_c)$  in the surface closure conditions, as discussed further by Lancz et al. (2017).

604 Shin and Hong (2015) have proposed a one-dimensional parameterization for the  
 605 CBL gray zone based on Eq. 9, but which gradually reduces the parameterized vertical  
 606 transport as model resolution increases. The local transports from small-scale eddies and  
 607 the sub-grid non-local transports are computed separately and reduced at different rates.  
 608 The non-local transport is formulated from three linear profiles which capture its three  
 609 most important roles: surface-layer cooling, mixed-layer heating, and entrainment at the  
 610 CBL top of air from aloft. Each of these profiles is constructed as a function of stabil-  
 611 ity parameters in the surface- and/or entrainment layers. The method is designed to re-  
 612 produce the total non-local turbulent transport, and the required sub-grid portion is com-  
 613 puted by multiplying an explicit grid-size dependent function which can also vary ac-  
 614 cording to the transported variable, the height (Honnert et al., 2011), and the stability  
 615 (Shin & Hong, 2013). The local transport is formulated as an eddy diffusivity, and is mul-  
 616 tiplied by a different grid-size dependent function (Shin & Hong, 2015). Both idealized  
 617 and real-case simulation results with the CBL gray-zone parameterization showed im-  
 618 provements over the use of the conventional unmodified parameterization at CBL gray-  
 619 zone resolutions.

620 Such changes, however, do not solve all the problems of the gray zone of turbulence.  
 621 The modified mass-flux, for example, remains based on horizontal homogeneity assump-  
 622 tions. Thus, it should be coupled with a local turbulence scheme that is itself adapted  
 623 to the CBL gray zone, especially over mountains where it does not produce enough tur-  
 624 bulent transports and can lead to unrealistic vertical velocities.

625 As noted in Section 1.2, the UK Met Office runs operational forecasts at gray zone  
 626 scales of 1.5 km and 333 m. Particularly in the latter case some of the large eddies re-  
 627 sponsible for much of the transport are resolved, but other turbulent motions are parti-  
 628 tially or completely unresolved and continue to require some non-local parameterization.  
 629 The approach has been to devise a pragmatic blending between mesoscale and LES pa-  
 630 rameterizations (Boutle et al., 2014). The former is provided by the Met Office bound-  
 631 ary layer scheme (Lock et al., 2000) (which is similar to Eq. 9 for a CBL) and the lat-  
 632 ter by a 3D Smagorinsky (Eq. 7) scheme. The blending is scale-dependent, being based  
 633 on the ratio of the grid scale to a diagnosed length scale characterising the turbulence.  
 634 The benefits of this blended parameterization in the UM are well illustrated by Boutle  
 635 et al. (2014), where a realistic stratocumulus case was simulated using horizontal grid  
 636 lengths from 100 m to 1 km, the turbulence changing from largely resolved to largely un-  
 637 resolved. However, the diffusive nature of the Smagorinsky scheme can result in the de-  
 638 layed spin up of non-local motions especially during the handover from the non-local mesoscale  
 639 to the Smagorinsky scheme in deepening CBLs, as shown in Efstathiou et al. (2016). Efstathiou  
 640 and Plant (2019) extended the blending approach by incorporating a scale-dependent  
 641 dynamic Smagorinsky scheme instead of the standard static Smagorinsky scheme. They  
 642 found some promising results in idealized simulations of an evolving CBL, particularly  
 643 in relation to the spin-up of resolved turbulence (cf. Section 3.3.2).

### 644 3.5 The gray zone of turbulence as a Rayleigh-Bénard convection prob- 645 lem

646 Zhou et al. (2014) examined the grid-dependent nature of gray-zone CBL simula-  
 647 tions using a mesoscale parameterization of turbulence. The analysis is based on the Rayleigh-  
 648 Bénard (RB) thermal instability framework, with the Rayleigh number ( $Ra$ ) redefined  
 649 by its turbulent counterpart

$$Ra = -P_{rT} \frac{N^2 H^4}{\nu_T^2}, \quad (11)$$

650 where  $P_{rT}$  is the turbulent Prandtl number,  $N$  ( $\text{s}^{-1}$ ) is the buoyancy frequency,  $\nu_T$  ( $\text{m}^2\text{s}^{-1}$ )  
 651 is the eddy viscosity, and  $H$  (m) is a length scale over which  $N$  is computed.  $H$  scales  
 652 with the boundary layer depth  $z_i$  (m). It is set to the surface layer depth (about  $0.1 z_i$ )  
 653 in Ching et al. (2014), and to  $z_i$  in Zhou et al. (2014). In extending the RB analysis to  
 654 the CBL, the effects of wind shear, which are mostly concentrated in the surface layer  
 655 and the entrainment zone, are ignored. Turbulent mixing terms are also linearized by  
 656 assuming an eddy-diffusion representation. Despite its simplicity, the RB framework is  
 657 useful for understanding model behaviors associated with conventional ABL schemes act-  
 658 ing on CBL gray zone grids. For example, the onset of convection in the resolved flow  
 659 was explained based on the RB framework. The onset depends on a critical value of  $Ra$   
 660 which is itself a function of grid spacing in the CBL gray zone. Sufficient instability in  
 661 the surface layer eventually leads to strong grid-scale convection after  $Ra$  has reached  
 662 its critical value.

663 The turbulent nature of grid-scale convection can mask mesoscale circulations, such  
 664 as a well-defined sea breeze. Ching et al. (2014) drew on the Rayleigh-Bénard framework  
 665 to develop a scheme based on the Rayleigh number which aims to suppress any convec-  
 666 tive motions in CBL gray zone simulations. Specifically the thermal diffusivity was mod-  
 667 ified in order to keep  $Ra$  below its critical value and so convective overturning remained  
 668 as a sub-filter process even at very fine grid lengths. This stands in contrast to the other  
 669 methods discussed in this paper.

### 670 3.6 Stochastic approach

671 As discussed in Section 2.4, scale adaptive modeling of transport in the boundary-  
 672 layer gray zone is intrinsically linked with representing stochastic behavior. Stochastic  
 673 backscatter techniques have a well-established value in improving LES simulations close  
 674 to the earth’s surface. The length scale of the dominant eddies close to the surface is con-  
 675 strained by the presence of the surface, so that  $l \sim z$ . It follows that the near-surface  
 676 flow may lie within the turbulence gray zone of  $l \sim \Delta$  even for situations in which the  
 677 turbulence in the interior of the flow is well resolved (Mason & Thomson, 1992; Wein-  
 678 brecht & Mason, 2008). The backscatter of energy from unresolved scales onto the grid  
 679 can improve turbulent statistics in such cases and has also proved helpful in the *near gray*  
 680 *zone*. A recent extension by O’Neill et al. (2015) allows for grid-independent spatial vari-  
 681 ations in the backscatter rate.

682 An important issue in the performance of gray-zone turbulence parameterizations,  
 683 as alluded to several times above, is a mechanism to initiate resolved-scale turbulent struc-  
 684 tures in an evolving flow. In reality turbulent length scales might be growing from sub-  
 685 grid to resolved scales but as the simulated growth may be overly slow, the explicit in-  
 686 clusion of some local near-grid-scale variability can prove useful. Backscatter, and other  
 687 stochastic methods, can provide such mechanisms. (An alternative may be to make the  
 688 low-level temperature profile unrealistically unstable by, for example, suppressing the non-  
 689 local flux, as shown in Efstathiou and Beare (2015).) The issue is most often discussed  
 690 in terms of the spin-up of resolved turbulence in time from an initial smooth field. How-  
 691 ever, similar issues also arise in transitioning to resolved turbulence downstream of the  
 692 smooth lateral boundary conditions that are usually imposed in numerical weather pre-  
 693 diction. Lateral boundary spin-up has received less attention in the literature to date,  
 694 but we note that some methods addressing the problem have been developed in the en-  
 695 gineering community, involving the injection of synthetic turbulence (e.g. Xie & Castro,  
 696 2008) and these ideas may provide a suitable remedy.

697 Various stochastic parameterization approaches have been developed for climate  
 698 models and ensemble-based numerical weather prediction as modifications to mesoscale  
 699 parameterization methods. To date, these have often been focused on the parameteri-  
 700 zation of diabatic processes, especially deep convection, and reviews of such techniques

are provided by Khouider et al. (2010); Palmer (2012) and Plant et al. (2015). Some of these ideas may also be applied in the CBL gray zone. Simple methods have included rescaling the parameterization tendencies by a random multiplicative factor or making random choices for some of the scheme parameters (Palmer, 2001). Alternatives have attempted to embed stochastic variability at a deeper level, within the sub-grid process description. A suitable starting point is to partition the total turbulent flux into contributions from multiple transporting elements, which may include information about size. Grid-scale adaptivity can then be achieved by size-filtering the population (Brast et al., 2018), while stochasticity can be represented in the element properties. A natural choice is to consider that a random number of elements may be found within a grid area (Leoncini et al., 2010; Plant & Craig, 2008) while others allow LES-informed random switching between distinct modes of turbulent heating (Dorrestijn et al., 2013) or random variability in the element/environment mixing rate (Suselj et al., 2014). The variables for which suitable spectra of elements have been constructed include the local thermodynamic state (Cheinet, 2003; Neggers et al., 2002, 2009), the mass flux carried by the elements (Plant & Craig, 2008; Sakradzija et al., 2014, 2016), or even size itself (Neggers et al., 2019; Park, 2014; T. M. Wagner & Graf, 2010).

A simple stochastic method has been implemented operationally in the Met Office UM turbulence-gray-zone configurations which draws on some of the above ideas. It can be considered as a simplified stochastic backscatter scheme where random boundary-layer temperature and humidity perturbations are applied to the smallest resolvable scale (taken to be 8 grid-lengths). The magnitude of the perturbations are designed to represent realistic boundary layer variability that would arise from a variety of poorly resolved processes at km-scale (not just boundary layer thermals but also surface heterogeneities and convection). The scheme also includes a time correlation of the perturbations on an approximate large-eddy turnover time scale. At present no attempt has been made to make these perturbations scale in a physically appropriate way, e.g. with the relative scale of the boundary-layer eddies to model resolution. Overall the scheme gives significant improvements to the initiation of small diurnally triggered convective showers over the UK and also improves spin-up of convective scale motions from the boundaries. Some other related approaches for introducing physically-based boundary-layer fluctuations are described by Muñoz-Esparza et al. (2014); Kober and Craig (2016); Leoncini et al. (2010).

Kealy et al. (2019) examined in more detail the impact of random boundary layer temperature perturbations on the spin-up of resolved turbulence at gray-zone resolutions. They found that the combination of imposed perturbations along with a scale-dependent sub-grid turbulence scheme has the most pronounced effect on the spin-up of resolved motion.

### 3.7 Grid refinement approach

Zhou et al. (2017) have proposed a rather different modeling methodology for CBL gray-zone simulations, based on refining the horizontal grid spacing in the surface layer (the bottom 10-15%). They adopt a two-way nesting technique to couple the simulation of the surface layer with that in the rest of the CBL. Since thermals in the CBL originate from the surface layer, the idea is that an improved representation of the surface layer should induce a good representation of the thermal population throughout the CBL. An LES turbulence closure is used in the surface layer and a mesoscale form of parameterization is adopted aloft. Zhou et al. (2018) demonstrate results which show substantial improvement of first and second order turbulent statistics, especially when horizontal resolution is refined up to half of the CBL depth (Zhou et al., 2017).

The grid refinement approach should be considered as a numerical method rather than a parameterization. In the high-resolution surface nest, assumptions behind ABL

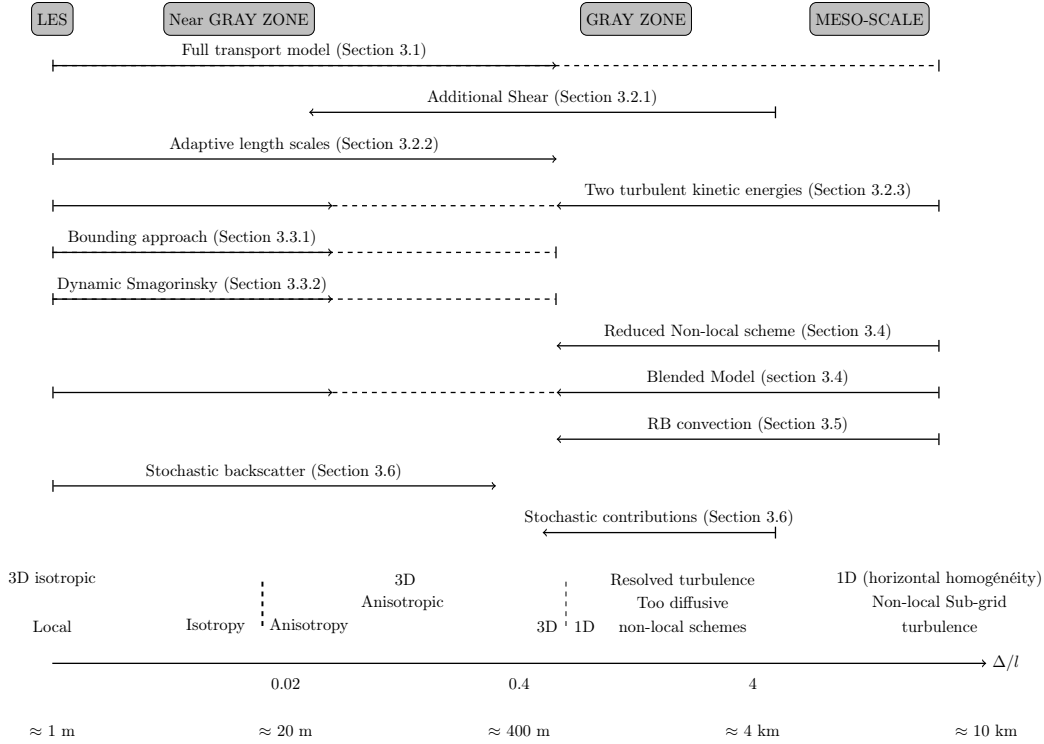


**Figure 8.** Schematic summarizing the relations between the various approaches that have been introduced and discussed. To simulate the turbulence in the gray zone, each method has a starting point in LES or mesoscale model and to a certain extent gets rid of the initial hypotheses. The dotted line shows where a parameterization family has no theoretical limit, but no application yet.

752 schemes are completely replaced by traditional LES assumptions (i.e. inertial sub-range  
 753 grid spacing and isotropic sub-grid turbulence). The grid refinement method does not  
 754 really differentiate grid spacings aloft, and can be applied as a general nesting method.  
 755 The method is of limited use to LES because the turbulent flows are already well resolved  
 756 in the CBL, although Sullivan et al. (1996) and Huq et al. (2014) did apply a similar method  
 757 with LES as an improved wall model to better resolve fine-scale surface-layer turbulence.  
 758 The method is also unnecessary for mesoscale models, because however well resolved the  
 759 thermals are in the nested high-resolution surface grids, they are not expected to have  
 760 any impact on the coarse mesoscale grids where they are entirely subgrid-scale.

761 **3.8 Summary and critical review**

762 Section 2 discusses the major challenges of modeling in the CBL gray zone. In the  
 763 LES regime, the subgrid-scale turbulence is small, homogeneous and isotropic. At the  
 764 near gray-zone, turbulence starts to become anisotropic (Section 2.4) and the possibil-  
 765 ity of some resolved-scale turbulence (Section 2.1) is a challenge, not least in producing  
 766 spin-up problems. In the gray-zone regime, the horizontal homogeneity hypothesis, usu-  
 767 ally used at mesoscales, is no longer valid (Section 2.4) and CBL thermals that are en-  
 768 tirely subgrid at the mesoscale (Section 2.2) are partly resolved. Figure 8 summarizes  
 769 the different regimes and the validity domains of the different parameterizations.

770 The experiences of performing CBL gray-zone simulations with conventional (LES  
 771 or mesoscale) parameterizations show that models are likely to fail to capture a correct

resolved turbulence or else to produce unrealistic over-energetic turbulent structures (Honnert et al., 2011). The behavior of models in the gray zone of turbulence depends on various physical factors (surface characteristics, topography, and time of day, among others) and also on the model specifications (such as the grid spacing, the diffusion, numerical damping, etc). Moreover, the model grid spacing itself can be a poor proxy of the actual model resolution (Ricard et al., 2013; Skamarock, 2004). In particular, the gray zone of turbulence cannot be limited to the hectometric scales: gray-zone issues can impact on modeling at both larger (Goger et al., 2018) and finer scales (Wyngaard, 2004).

Nonetheless, there does seem to be a critical core of new ideas emerging that is well worth pursuing in sub-kilometer simulations. No parameterization is created *ex nihilo*. Historically, LES and mesoscale schemes have drawn upon assumptions and simplifications that are informed by our understandings of the atmospheric boundary layer. For instance, most mesoscale schemes assume that turbulent fluxes are horizontally homogeneous so that only the vertical flux needs to be parameterized. On the other hand, most LES schemes assume that sub-grid turbulence is isotropic. The subgrid flux is characterized by a single mixing length when an eddy viscosity model is employed.

Figure 8 shows two categories of scheme. One category treats the gray zone of turbulence by starting from mesoscale approaches and attempt to adapt and extend them for higher resolution applications (mass-flux modifications and Shin and Hong (2015), RB representation and most of the stochastic parameterizations). These schemes typically aim to reduce the non-local subgrid turbulence, but remain focused on a vertical 1D representation of the CBL. Some of these schemes operate by blending LES and mesoscale formulations, including the two turbulence kinetic energy approach (Bhattacharya & Stevens, 2016) and the blended model of (Boutle et al., 2014). The blended approaches seem able to produce scale-adapted subgrid CBL thermals, as well as LES isotropic turbulence when necessary. However, there is as yet no good evidence that they can capture the anisotropic character of the turbulence in the near gray zone regime. The incorporation of additional wind shear terms in a TKE scheme, as in (Goger et al., 2018), may compensate for the lack of 3D turbulence in the gray zone, but it does not produce the limiting forms of behavior of 1D CBL thermals at the mesoscale or a 3D isotropic scheme in LES. The other major category attempts to treat the gray zone of turbulence as essentially “coarse LES” by adapting and extending LES turbulence models into the gray-zone regime (full transport model, all adaptations of the mixing length, bounding model and dynamical Smagorinsky). Such schemes have had some successes, especially in extending from the LES, isotropic, mainly-resolved turbulence regime into the near gray-zone anisotropic-turbulence region, but they cannot represent non-local turbulence typical of the CBL at the mesoscale.

Although most of the parameterizations that have been developed so far cannot be seamlessly used from LES to the mesoscales, they do provide some interesting clues towards solving practical problems in the gray zone of turbulence. Some promising results have emerged from both major categories. Some simple blending/hybrid schemes using non-local turbulence (Boutle et al., 2014; Efstathiou & Plant, 2019; Shin & Hong, 2015), TKE (Ito et al., 2015; Zhang et al., 2018) or mass-flux approaches (Honnert et al., 2016) may significantly improve the representation of first-order quantities and turbulence statistics in the CBL gray zone.

## 4 Discussions

Modeling within the CBL gray zone is increasingly becoming seen as necessary for near future operational use because there is a growing demand for higher resolution forecasting, especially for the prediction of high-impact weather events. A wide range of novel approaches have been presented (Section 3) in this article incorporating various new parameterization ideas to address the challenges of the CBL gray zone. Moreover, an increasing number of researchers are actively working on the topic. Thus, the turbulence

823 gray zone has clearly become a hot topic in atmospheric modeling. However, key ques-  
 824 tions remain.

#### 825 **4.1 Is the gray zone of turbulence stalling the improvement of atmo-** 826 **spheric modeling?**

827 Our review has shown that most of the gray-zone turbulence studies to date have  
 828 been based on idealized or real but relatively simple well-known cases over homogeneous  
 829 surfaces (e.g. the Wangara case study). Some caution is therefore needed. In order to  
 830 develop atmospheric modeling we require not just that there is an appropriate treatment  
 831 of turbulent motions in the gray zone but also that their treatment should enable the  
 832 correct interactions with other atmospheric processes. These points are discussed in Sec-  
 833 tion 2.6 and are highlighted by LeMone et al. (2010) or J. S. Wagner et al. (2014) for  
 834 example. However, there are also well-documented cases that clearly benefit from im-  
 835 proving resolution into the gray zone of turbulence, despite potential issues with sub-  
 836 grid scale turbulence parameterization. This can be seen in the simulations of Warren  
 837 et al. (2014) for a slow-moving organized convective system over a complex terrain area  
 838 in southwest England.

839 Most scale-aware gray-zone schemes for the CBL have been developed with a focus  
 840 on cloud-free conditions or with shallow cumulus clouds. It is much less clear how  
 841 many of the schemes would perform in deep moist convection environments, including  
 842 organized systems or tropical cyclones. It is also less clear how they might couple to synoptic-  
 843 scale motions (Section 2.6). A useful study from this perspective is that of Green and  
 844 Zhang (2015) who investigated the partition between resolved and sub-grid turbulent fluxes  
 845 in turbulence gray-zone simulations of hurricane Katrina. In their simulations, the par-  
 846 titioning and the character of the resolved turbulent structures varied significant with  
 847 the resolution, but the system’s intensity was not affected because the total turbulent  
 848 fluxes remained almost the same. Other case studies of other phenomena with other ap-  
 849 proaches to the gray zone of turbulence would clearly be valuable.

850 The complexity of partially-resolved structures in the gray-zone boundary layer and  
 851 the feedbacks between resolved and sub-grid dynamics during deep convective cloud de-  
 852 velopment are not yet understood. Pronounced sensitivity to turbulent mixing in sub-  
 853 kilometer simulations of deep convection has been identified in a number of recent stud-  
 854 ies. Verrelle et al. (2015) showed that insufficient mixing led to strong undiluted ther-  
 855 mals and unrealistic resolved TKE in a super-cell simulation. In Hanley et al. (2014),  
 856 simulated deep clouds were found to exhibit small features compared to radar observa-  
 857 tions, although their representation could be somewhat improved by increasing the sub-  
 858 grid turbulence mixing length. Moreover, Verrelle et al. (2017) identified the presence  
 859 of non-local structures in deep clouds that can pose significant challenges to conventional  
 860 mixing schemes. Ito et al. (2017) examined a number of heavy rainfall cases and found  
 861 that the rate of improvement in the skill of the forecasts became progressively smaller  
 862 for further increases of horizontal resolution into the sub-kilometric regime. Although  
 863 their simulations seemed to be relatively insensitive to the CBL representation, the re-  
 864 sults do indicate that interactions of the near-grid scale with the larger scale environ-  
 865 ment, and with other processes, might still be important in the gray zone of turbulence.

866 An important context for these findings is the resolution required for the represen-  
 867 tation of deep convective clouds. There is a convective gray zone associated with such  
 868 clouds at grid spacings of around 1 – 10 km. So called “convection permitting” simu-  
 869 lations with the convection parameterization switched off have been shown to yield some  
 870 significant benefits for  $\Delta x < 5$  km (Roberts & Lean, 2008). However one would not ex-  
 871 pect the deep clouds to be well represented on a numerical grid unless one can adequately  
 872 resolve the turbulent mixing processes at the cloud edges. These have a scale of  $\sim 100$  m  
 873 (Craig & Dornbrack, 2008), so improvements in modeling explicit deep convection might

874 prove modest until those grid length scales are reached, *unless* a better parameterization  
 875 of turbulent mixing processes can be introduced.

876 As illustrated by Stirling and Petch (2004) and Kealy et al. (2019), the impact of  
 877 small-scale boundary-layer variability is important for an accurate representation of the  
 878 diurnal cycle of convection in the turbulence gray zone, not least for the timing of deep  
 879 cloud initiation. This point encourages further development of stochastic approaches and  
 880 improvement can reasonably be anticipated from imposing appropriate small-scale vari-  
 881 ability in the CBL.

## 882 **4.2 Should resolved convective motion be allowed in the turbulence gray** 883 **zone?**

884 Ching et al. (2014) argue that any partly-resolved turbulent motions in gray-zone  
 885 ABL simulations are not realistic and should be damped. Since the simulations are not  
 886 in the LES converging regime and the results depend heavily on the imposed dissipation,  
 887 they should not be trusted. Hence, these authors pursue an ensemble-average approach  
 888 to the model filter operation, in which their gray-zone ABL simulations are valued for  
 889 producing improved numerical accuracy for a mesoscale modeling approach (cf. Mason  
 890 & Brown, 1999). The authors showed an example of noisy resolved motions that masked  
 891 the lake-breeze field. However, they do recognize the importance of resolved convective  
 892 structures in the CBL for the triggering of deep convection, as discussed in the previ-  
 893 ous subsection.

894 The initiation of resolved motion in gray-zone ABL simulations is generally con-  
 895 sidered to be a valued aspect for the majority of gray-zone ABL studies and for oper-  
 896 ational atmospheric models. By allowing some partially-resolved convective overturn-  
 897 ing motion, most modelers are (conceptually at least) following a spatially-filtered ap-  
 898 proach in which an *appropriate* level of variability near to the filter scale is considered  
 899 to be desirable. It should be stressed that this is also the view taken by coarse-graining  
 900 studies and in simulation strategies developed from those.

## 901 **4.3 Testing models in a realistic set-up - The Gray Zone Project**

902 The Gray Zone Project promotes international collaborations and community ac-  
 903 tivities in the development of scale-aware deep and shallow convection and boundary-  
 904 layer parameterizations and focuses on grid lengths of about 200 m to 10 km. It has been  
 905 initiated by WGNE (Working Group on Numerical Experimentation) and the GEWEX  
 906 (Global Energy and Water Exchanges) Global Atmosphere System Studies.

907 A first phase of the Gray Zone Project examined the simulation of a maritime cold  
 908 air outbreak that was observed during a field campaign (Field et al., 2014). Model in-  
 909 tercomparisons have been reported for simulations with global models (Tomassini et al.,  
 910 2016), limited-area models Field et al. (2017) and large-eddy simulations (de Roode et  
 911 al., 2019). Model resolutions were systematically varied in order to explore their behav-  
 912 iors across a range of spatial scales, and results were compared to the observations. A  
 913 second phase of the project is now being planned and will investigate shallow cumulus  
 914 clouds at turbulence gray-zone resolutions as part of the EUREC4A project in 2020 (Elucidating  
 915 the role of clouds-circulation coupling in climate, Bony et al., 2017) and also the tran-  
 916 sition from shallow to deep convective clouds over the eastern tropical Atlantic based on  
 917 the GATE field campaign (Global Atmospheric Research Program’s Atlantic Tropical  
 918 Experiment, Kuettner, 1974).



#### 919 4.4 Prognostic adaptive schemes the way forward?

920 Most proposed methodologies in the boundary-layer gray zone have either LES or  
 921 mesoscale parameterizations as their starting point. However, various mesoscale param-  
 922 eterizations based on prognostic equations do exist (e.g. Lappen & Randall, 2001; Tan  
 923 et al., 2018), and since these tend to be more adaptive to the resolved flow, they may  
 924 be worth more attention in terms of developing extensions for the gray zone of turbu-  
 925 lence. Such mesoscale parameterizations are often designed with an assumption that the  
 926 thermal fraction is assumed small, which is a defect in the gray zone of turbulence. Mod-  
 927 ifications such as those in Honnert et al. (2016) to introduce a scale-aware thermal area  
 928 fraction may therefore be necessary in extending their use. A related starting point could  
 929 also be that of Thuburn et al. (2018), who recently proposed a two-fluid theoretical frame-  
 930 work for the representation of convection in models, using coupled prognostic primitive  
 931 equations for both the coherent eddy structures (convective plumes) and their environ-  
 932 ment.

933 An approach that seems to be able to bridge the gap between the LES and the mesoscale  
 934 limits, is the full transport model of Wyngaard (2004). Nevertheless, solving several prog-  
 935 nostic higher-order equations, involving several terms that require further closure assump-  
 936 tions and parameters, can be computationally expensive. Linear algebra closure mod-  
 937 els such as Lazeroms et al. (2016) could offer a potential route forwards to reducing com-  
 938 putational costs while retaining the tensor representation of the fluxes that is at the core  
 939 of the approach. In either case, the dynamic modeling technique of filtering at multiple  
 940 scales (Bou-Zeid et al., 2005; Chow et al., 2005) can be used to determine the necessary  
 941 length scales and tuning parameters, thereby making such schemes not only scale-aware  
 942 but also flow-dependent. Dynamic calculation of length scales in an evolving CBL has  
 943 been shown to be beneficial for the CBL gray zone (Efstathiou et al., 2018; Efstathiou  
 944 & Plant, 2019).

945 It is clear that special care needs to be taken in the gray zone of turbulence for the  
 946 representation of horizontal fluxes (Zhou et al., 2017). The conventional 2D Smagorin-  
 947 sky adaptation for horizontal mixing has been shown to be inappropriate in the repre-  
 948 sentation of CBL mixing (Ito et al., 2014; Zhou et al., 2017). A recent scale-aware rep-  
 949 resentation of horizontal diffusion from Zhang et al. (2018), based on Honnert et al. (2011)  
 950 and using the blending approach of Boutle et al. (2014), has shown promising results.

## 951 5 Conclusions

952 We have reviewed the current state of a newly-emerged research area in the numer-  
 953 ical modeling of geophysical flows and discussed the significant challenges that arise for  
 954 the atmospheric modeling community. Numerical models are now moving towards sub-  
 955 kilometer grid spacings at which they produce partially-resolved turbulent structures.  
 956 As a result in the “gray zone” of turbulence, the fundamental assumptions underpinning  
 957 our conventional treatments of sub-grid scale variability are no longer valid. Furthermore,  
 958 at CBL gray-zone resolutions the resolved scale variability becomes highly dependent on  
 959 the representation of sub-grid motion that in turn can compromise the accuracy and value  
 960 of the numerical model simulations.

961 A model’s horizontal grid spacing cannot by itself determine the onset of the CBL  
 962 gray zone or explain the transition of the TKE and heat and moisture fluxes from the  
 963 LES to the mesoscale limit. The key to describing the transition is to consider the rel-  
 964 ative extent of the dominant turbulence length scales compared to the effective grid spac-  
 965 ing. This means that different structures, whether these are CBL thermals or clouds at  
 966 the top of the ABL, might be in different resolution regimes especially as they evolve over  
 967 time (similar to Fig. 6). It also means that one should take into account the imposed  
 968 dissipation from the numerical methods in use, which can damp or smooth the resolved

969 field. The interplay of numerical and "physical" diffusion (from the turbulence param-  
 970 eterization) will determine the effective resolution of an atmospheric model; i.e. its abil-  
 971 ity to partially resolve features at the limits of its grid resolution (Skamarock, 2004).

972 The proposed gray-zone CBL parameterization schemes in the literature, as pre-  
 973 sented here, are largely based on two approaches: treating the gray zone of turbulence  
 974 as either a coarse LES or a high-resolution mesoscale model depending on the starting  
 975 point of each parameterization. However, there are some approaches that attempt to avoid  
 976 the bulk of the gray zone of turbulence, either by increasing the horizontal resolution in  
 977 certain parts of the CBL or by filtering out any turbulent motions. The latter approach  
 978 considers the simulation to belong the mesoscale resolution regime where all of the tur-  
 979 bulent transfer is parameterized in an ensemble-average sense. Even though many of the  
 980 schemes considered show certain merits and benefits in the gray zone of turbulence, most  
 981 of them have been tested in idealized settings. As a next step more comprehensive stud-  
 982 ies are needed using realistic case studies to identify the interactions of partially-resolved  
 983 turbulent mixing with deep convective clouds and with the larger scale circulations.

984 The full turbulent transfer equations should, at least in principle, be able to han-  
 985 dle the transition of turbulent transfer from well resolved to fully parameterized. How-  
 986 ever, solving the full turbulent transport equations would be computationally expensive  
 987 and suitable closure assumptions would be needed, perhaps depending on the level of in-  
 988 formation that is available from the resolved motions. As this approach may not be prac-  
 989 tical, even with the available computing power, the anisotropic production terms in the  
 990 transport equations might be usefully retained in various simplified ways.

991 It is very clear that the existence of the turbulence gray zone has important im-  
 992 plications and consequences for atmospheric modeling and for the future of numerical  
 993 weather prediction in particular. Recent studies, such as those discussed in Section 4,  
 994 have demonstrated that at sub-kilometer grid spacings increasing convergence with in-  
 995 creasing grid resolution is not guaranteed, especially in simulations with deep convec-  
 996 tion. However, the full extent of the impact of partially resolved turbulent flow on the  
 997 actual performance of weather forecasting needs to be further investigated. This is partly  
 998 due to the fact that some of the feedbacks between the turbulent mixing in the CBL and  
 999 synoptic-scale systems are not yet well understood. Nevertheless, the refined resolution  
 1000 can still prove to be beneficial, especially when it is combined with better representa-  
 1001 tion of topography and surface heterogeneity and especially in cases with strong large-  
 1002 scale forcing.

1003 Although this article has been focused on the CBL gray zone and atmospheric sim-  
 1004 ulations, other aspects of geophysical fluid flow modeling experience their own gray zone.  
 1005 The representation of any important physical phenomenon with a length scale of the same  
 1006 order as the grid spacing is liable to be problematic in numerical simulations. Such a sit-  
 1007 uation is clearly undesirable but sometimes cannot be avoided, due to finite computa-  
 1008 tional limitations or else because the phenomenon itself covers a range of scales. The CBL  
 1009 gray zone is *relatively* simple in various respects, the dominant turbulent structures be-  
 1010 ing well understood and having a well-defined length scale dictated by the CBL depth.  
 1011 Thus, it provides a good base case for the study of possible methods for treating gray  
 1012 zone motions in geophysical flows more generally. Promising approaches to gray zones  
 1013 may be more easily identified in this setting, and conversely, it seems difficult to imag-  
 1014 ine that approaches performing poorly for the CBL gray zone would somehow work well  
 1015 in other, more complex settings.

## 1016 Appendix A The full transport equations

In Section 3.1 a tensor form of the eddy diffusivity was presented. Following Wyngaard  
 (2004), this may be derived from the scalar-flux transport equation. The sub-grid flux

of a conserved scalar field  $c$  in the  $i$  direction is denoted  $f_i = \overline{c\bar{u}_i} - \bar{c} \bar{u}_i$  where the overbar is a spatial filter, and it evolves as (Wyngaard, 2004):

$$\frac{\partial f_i}{\partial t} + \bar{u}_j \frac{\partial f_i}{\partial x_j} = -f_j \frac{\partial \bar{u}_i}{\partial x_j} - \tau_{ij} \frac{\partial \bar{c}}{\partial x_j} + \text{PT} + \text{FLXDIV}, \quad (\text{A1})$$

1017 The first two terms on the right hand side are production terms, the first (tilting term)  
 1018 representing the stretching and "tilting" of turbulent eddies and the second represent-  
 1019 ing the interaction of turbulent fluxes (Reynolds stresses,  $\tau_{ij}$ ) with the scalar gradient  
 1020 (gradient term). Other terms express the pressure – scalar interactions (PT) and the di-  
 1021 vergence of the sub-grid flux of  $f_i$  (FLXDIV). The flux divergence terms contain higher  
 1022 order contributions that express the sub-grid turbulent transport of  $f_i$ . PT acts as a prin-  
 1023 cipal sink for the scalar flux and can be parameterized as  $-f_i/T$  in its simplest linear  
 1024 form, with  $T$  representing a characteristic time scale of the sub-grid turbulence.

1025 Wyngaard (2004) proposed a model for the sub-grid scalar fluxes that is obtained  
 1026 by retaining the first two production terms in Eq. A1, assuming a steady state, and bal-  
 1027 ancing the production with the pressure terms. The model is given by:

$$1028 \quad f_i = -T \left( f_j \frac{\partial \bar{u}_i}{\partial x_j} + \tau_{ij} \frac{\partial \bar{c}}{\partial x_j} \right). \quad (\text{A2})$$

1029 Although Eq. A2 expresses an algebraic model, it would be entirely straightforward to  
 1030 retain a prognostic form based on Eq. A1.

1031 Dropping the tilting terms and retaining only the gradient production terms in the  
 1032 direction of the flux (isotropic gradient production), Eq. A2 reduces to:

$$1033 \quad f_i = -T \tau_{ii} \frac{\partial \bar{c}}{\partial x_i} = -K_c \frac{\partial \bar{c}}{\partial x_i}. \quad (\text{A3})$$

1034 This corresponds to the down-gradient diffusion model that is commonly used as a ba-  
 1035 sis for turbulence parameterization in both LES closures and mesoscale ABL schemes.  
 1036  $K_c = T \tau_{ii}$  is the eddy diffusivity. Without these additional assumptions, the formal so-  
 1037 lution of Eq. A2 is given by Eq. 2 (Wyngaard, 2004):

$$1038 \quad f_i = -K_{ij} \frac{\partial \bar{c}}{\partial x_j} \quad (\text{A4})$$

1039 where  $K_{ij}$  is a tensor form of the eddy diffusivity which is a function of  $T$ , the shear ten-  
 1040 sor  $\partial \bar{u}_i / \partial x_j$  and  $\tau_{ij}$ .

## 1041 Glossary

1042 **Atmospheric Boundary layer** The bottom layer of the atmosphere that is in con-  
 1043 tact with the surface of the earth.

1044 **Free Troposphere** The part of the Earth's troposphere which excludes the boundary  
 1045 layer. Turbulence in the boundary layer is ubiquitous but in the free troposphere  
 1046 is produced only sporadically, by mechanical forcing in regions of pronounced wind  
 1047 shear or thermally inside convective clouds.

1048 **Backscatter** Energy transfers in turbulent three-dimensional fluid motions occur to both  
 1049 larger and smaller spatial scales. The net transfer within the inertial subrange is  
 1050 downscale but the backscatter refers to the upscale component of energy trans-  
 1051 fer, from subgrid-scale to resolved motions.

1052 **Baroclinic waves** Synoptic-scale disturbances that grow in the mid-latitudes due to  
 1053 baroclinic instability and which are responsible for the development of weather  
 1054 systems.

1055 **Deep Clouds** Clouds with predominantly vertical development that form as a result  
 1056 of deep convection in the troposphere. They may extend from the top of the bound-  
 1057 ary layer towards the upper troposphere (cumulus congestus) or as far as the tropopause

- 1058 (cumulonimbus). Such clouds may be associated with thunderstorms, heavy rain-  
 1059 fall and hail.
- 1060 **Large-Eddy Simulation** A three-dimensional numerical simulation of turbulence, in  
 1061 which the largest eddies are explicitly resolved, while the effects of subgrid-scale  
 1062 eddies in the inertial subrange are parameterized.
- 1063 **Large/synoptic-scale** The scales of the general atmospheric circulation related to the  
 1064 high-tropospheric long-wave patterns.
- 1065 **Low-level jet** A jet of wind that appears in the boundary layer.
- 1066 **Mesoscale** Refers to atmospheric phenomena having horizontal scales ranging from a  
 1067 few to several tens of kilometers, including thunderstorms, squall lines and topographically-  
 1068 induced circulations such as mountain waves, mountain and valley breezes as well  
 1069 as sea and land breezes.
- 1070 **Parameterization** The representation, in a dynamic model, of physical effects in terms  
 1071 of admittedly oversimplified parameters, rather than realistically requiring such  
 1072 effects to be consequences of the dynamics of the system (from American Mete-  
 1073 orological Society Glossary).
- 1074 **Shallow Clouds** Low-level, usually non-precipitating, clouds which may be considered  
 1075 to form part of the ABL. Cumulus and stratocumulus are forms of shallow con-  
 1076 vective clouds.
- 1077 **Troposphere** That portion of the atmosphere where most weather occurs and which  
 1078 extends from the Earth’s surface to a sharp temperature inversion at the tropopause,  
 1079 between 10 and 20 km aloft.
- 1080 **Surface Layer** The lowest 10–15% of the atmospheric boundary layer where first or-  
 1081 der quantities such as wind and temperature follow an approximately logarithmic  
 1082 profile and turbulent fluxes may be considered almost constant.
- 1083 **Non-local turbulence** A term used in the context of 1D mesoscale parameterizations  
 1084 to refer to coherent turbulent structures that typically extend to the full depth  
 1085 of the turbulent layer. In the CBL, non-local turbulence is associated with buoy-  
 1086 ant thermals.

## 1087 Acronyms

- 1088 **ABL** Atmospheric Boundary Layer  
 1089 **CBL** Convective (Atmospheric) Boundary Layer  
 1090 **COSMO** Consortium for Small-Scale Modeling  
 1091 **GEWEX** Global Energy and Water Exchanges Global  
 1092 **LEM** Met Office Large Eddy Model  
 1093 **LES** Large Eddy Simulation  
 1094 **MYNN** Mellor-Yamada-Nakanishi-Niino model  
 1095 **NWP** Numerical Weather Prediction  
 1096 **RB** Rayleigh-Bénard  
 1097 **TKE** Turbulent Kinetic Energy  
 1098 **VLES** Very Large-Eddy Simulation  
 1099 **WGNE** Working Group on Numerical Experimentation  
 1100 **WRF** Weather Research and Forecasting

## 1101 Notation

- 1102  $c$  a conserved scalar.  
 1103  $c_u$  value of  $c$  inside the mass-flux thermal plume  
 1104  $\bar{c}$  mean value of  $c$   
 1105  $C_c$  a constant value for a given scalar  $c$

1106	$C_s$ Smagorinsky coefficient
1107	$\Delta$ grid spacing, model resolution
1108	$\Delta x$ model horizontal grid spacing
1109	$\Delta z$ model vertical spacing
1110	$e$ TKE
1111	$e_{\text{sgs}}$ subgrid-scale TKE
1112	$e_{\text{res}}$ resolved TKE
1113	$e_{\text{tot}}$ total (resolved plus subgrid-scale) TKE
1114	$f_i$ sub-grid scalar flux
1115	$\gamma$ counter-gradient term
1116	$H$ a length scale over which $N$ is computed
1117	$k$ wave number
1118	$k_{d,\text{eff}}$ dissipation wave-number in Beare (2014)
1119	$k_d$ dissipation wave-number
1120	$k_0, k_1$ wave-number limits in Beare (2014)
1121	$K_c$ the eddy diffusivity associated with the conserved variable $c$
1122	$K_{ij}$ a tensor form of the eddy diffusivity
1123	$l$ length scale of the dominant energy containing structures
1124	$l_m$ mixing length used in a TKE based parameterization
1125	$l_t$ Smagorinsky mixing length scale
1126	$l_d$ dissipation length scale
1127	$\nu_T$ the eddy viscosity
1128	$M_u$ mass-flux of ABL thermals
1129	$\text{Pr}$ Prandtl number
1130	$\text{Pr}_T$ turbulent Prandtl number
1131	$\text{Ra}$ Rayleigh number
1132	$\tau_{ij}$ Reynolds stress
1133	$S_e$ TKE power spectrum
1134	$T$ time scale for sub-grid turbulence
1135	$\theta$ potential temperature
1136	$u$ a wind component
1137	$w$ vertical velocity
1138	$z_c$ depth of the cloud layer
1139	$z_i$ CBL height
1140	$z$ altitude

## 1141 Acknowledgments

1142 This article is a review paper : Data were not used, nor created for this research

## 1143 References

- 1144 Adamson, D. S., Belcher, S. E., Hoskins, B. J., & Plant, R. S. (2006). Boundary-  
 1145 layer friction in midlatitude cyclones. *Q. J. R. Meteorol. Soc.*, *132*, 101-124.
- 1146 Arakawa, A., Jung, J.-H., & Wu, C.-M. (2011). Toward unification of the multiscale  
 1147 modeling of the atmosphere. *Atmos. Chem. Phys.*, *11*(8), 3731–3742.
- 1148 Arakawa, A., & Wu, C.-M. (2013). A unified representation of deep moist convection  
 1149 in numerical modeling of the atmosphere. Part I. *J. Atmos. Sci.*, *70*(7), 1977-  
 1150 1992.
- 1151 Arnold, D., Morton, D., Schicker, I., Seibert, P., Rotach, M., Horvath, K., ...  
 1152 Schneider, S. (2012, 02). High resolution modelling in complex terrain. *Report*

- 1153           on the *HiRCoT 2012 Workshop, Vienna*.
- 1154   Arnold, D., Morton, D., Schicker, I., Seibert, P., Rotach, M., Horvath, K., ...
- 1155        Schneider, S. (2014). Issues in high-resolution atmospheric modeling in
- 1156        complex terrain - the HiRCoT workshop. *Croat. Meteor. J.*, *47*, 311.
- 1157   Basu, S., Vinuesa, J.-F., & Swift, A. (2008). Dynamic LES modeling of a diurnal cy-
- 1158        cle. *J. Appl. Meteorol. Climatol.*, *47*, 1156-1174.
- 1159   Beare, R. J. (2014). A length scale defining partially-resolved boundary-layer turbu-
- 1160        lence simulations. *Boundary-Layer Meteorol.*, *151*, 39-55.
- 1161   Beljaars, A. C. M., Brown, A. R., & Wood, N. (2004). A new parametrization of
- 1162        turbulent orographic form drag. *Q. J. R. Meteorol. Soc.*, *130*(599), 1327-1347.
- 1163   Bengtsson, L., Tijm, S., Vana, F., & Svensson, G. (2012). Impact of flow-dependent
- 1164        horizontal diffusion on resolved convection in AROME. *J. Appl. Meteorol. Cli-*
- 1165        *matol.*, *51*(1), 54-67.
- 1166   Bhattacharya, R., & Stevens, B. (2016). A two turbulence kinetic energy model as
- 1167        a scale adaptive approach to modeling the planetary boundary layer. *J. Adv.*
- 1168        *Model. Earth Syst.*, *8*:1, 224-243.
- 1169   Bony, S., Stevens, B., Ament, F., Bigorre, S., Chazette, P., Crewell, S., ... Wirth,
- 1170        M. (2017). EUREC4A: A field campaign to elucidate the couplings between
- 1171        clouds, convection and circulation. *Surveys in Geophysics*, *38*, 1529-1568.
- 1172   Boutle, I. A., Belcher, S. E., & Plant, R. S. (2015). Friction in mid-latitude cyclones:
- 1173        an Ekman-PV mechanism. *Atmos. Sci. Lett.*, *16*, 103-109.
- 1174   Boutle, I. A., Eyre, J. E. J., & Lock, A. P. (2014). Seamless stratocumulus simula-
- 1175        tion across the turbulent grey zone. *Mon. Wea. Rev.*, *142*, 1655-1668.
- 1176   Bou-Zeid, E., Meneveau, C., & Parlange, M. (2005). A scale-dependent Lagrangian
- 1177        dynamic model for large eddy simulation of complex turbulent flows. *Phys.*
- 1178        *Fluids*, *17*(2), 025105. doi: 10.1063/1.1839152
- 1179   Brast, M., Schemann, V., & Neggers, R. A. J. (2018). Investigating the scale-
- 1180        adaptivity of a size-filtered mass flux parameterization in the gray zone of
- 1181        shallow cumulus convection. *J. Atmos. Sci.*, *75*, 1195-1214.
- 1182   Brown, A. R., Cederwall, R. T., Chlond, A., Duynkerke, P. G., Golaz, J.-C.,
- 1183        Khairoutdinov, M., ... Stevens, B. (2002). Large-eddy simulation of the
- 1184        diurnal cycle of shallow cumulus convection over land. *Q. J. R. Meteorol. Soc.*,
- 1185        *128*, 1075-1093.
- 1186   Bryan, G. H., & Morrison, H. (2012). Sensitivity of a simulated squall line to hori-
- 1187        zontal resolution and parameterization of microphysics. *Mon. Wea. Rev.*, *140*,
- 1188        202-225.
- 1189   Cheinet, S. (2003). A Multiple Mass-Flux Parameterization for the Surface-
- 1190        Generated Convection. Part I: Dry Plumes. *J. Atmos. Sci.*, *60*, 2313-2327.
- 1191   Chen, R., & Tomassini, L. (2015). The role of moisture in summertime low-level jet
- 1192        formation and associated rainfall over the East Asian monsoon region. *J. At-*
- 1193        *mos. Sci.*, *72*, 3871-3890.
- 1194   Ching, J., Rotunno, R., LeMone, M., Martilli, A., Kosovic, B., Jimenez, P. A., &
- 1195        Dudhia, J. (2014). Convectively induced secondary circulations in fine-grid
- 1196        mesoscale numerical weather prediction models. *Mon. Wea. Rev.*, *142*:9.
- 1197   Chow, F. K., Street, R. L., Xue, M., & Ferziger, J. H. (2005). Explicit filtering and
- 1198        reconstruction turbulence modeling for large-eddy simulation of neutral bound-
- 1199        ary layer flow. *J. Atmos. Sci.*, *62*(7), 2058-2077. doi: 10.1175/JAS3456.1
- 1200   Clarke, R. H., Dyer, A. J., Reid, D. G., & Troup, A. J. (1971). The Wangara exper-
- 1201        iment: Boundary layer data. *Division Meteorological Physics Paper, CSIRO*,
- 1202        *19*, Australia.
- 1203   Couvreur, F., Guichard, F., Redelsperger, J.-L., Kiemle, C., Masson, V., Lafore,
- 1204        J.-P., & Flamant, C. (2005). Water vapour variability within a convective
- 1205        boundary-layer assessed by large-eddy simulations and IHOP2002 observations.
- 1206        *Q. J. R. Meteorol. Soc.*, *131*, 2665-2693.
- 1207   Couvreur, F., Hourdin, F., & Rio, C. (2010). Resolved versus parametrized

- 1208 boundary-layer plumes. Part I: A parametrization-oriented conditional sam-  
 1209 pling in large-eddy simulations. *Boundary-layer Meteorol.*, *134*(3), 441–458.
- 1210 Craig, G. C., & Dornbrack, A. (2008). Entrainment in cumulus clouds: What resolu-  
 1211 tion is cloud-resolving? *J. Atmos. Sci.*, *65*, 3978–3988.
- 1212 De Roode, S. R., Duynkerke, P. G., & Jonker, H. J. J. (2004). Large-eddy simula-  
 1213 tion : How large is large enough? *J. Atmos. Sci.*, *61*, 403–421.
- 1214 de Roode, S. R., Frederikse, T., Siebesma, A. P., Ackerman, A. S., Field, P. R., Hill,  
 1215 A., . . . L. Tomassini (2019). Turbulent transport in the grey zone: A large-  
 1216 eddy simulation intercomparison study of the CONSTRAIN cold air outbreak  
 1217 case. *J. Adv. Model. Earth Syst.*, *11*, 597–623.
- 1218 Deardorff, J. W. (1972). Theoretical expression for the counter gradient vertical flux.  
 1219 *J. Geophys. Res.*, *77*, 5900–5904.
- 1220 Deardorff, J. W. (1980). Stratocumulus-capped mixed layers derived from a three-  
 1221 dimensional model. *Boundary-Layer Meteorol.*, *18*, 495–527.
- 1222 Dorrestijn, J., Crommelin, D. T., Siebesma, A. P., & Jonker, H. J. J. (2013).  
 1223 Stochastic parameterization of shallow cumulus convection estimated from  
 1224 high-resolution model data. *Theor. Comp. Fluid Dyn.*, *27*(1-2), 133–148.  
 1225 Retrieved from <http://dx.doi.org/10.1007/s00162-012-0281-y> doi:  
 1226 10.1007/s00162-012-0281-y
- 1227 Duffourg, F., Nuissier, O., Ducrocq, V., Flamant, C., Chazette, P., Delanoé, J., . . .  
 1228 Bock, O. (2016). Offshore deep convection initiation and maintenance dur-  
 1229 ing HyMeX IOP16a heavy precipitation event. *Q. J. R. Meteorol. Soc.*, *142*,  
 1230 259274.
- 1231 Efstathiou, G. A., & Beare, R. J. (2015). Quantifying and improving sub-grid diffu-  
 1232 sion in the boundary-layer grey zone. *Q. J. R. Meteorol. Soc.*, *141*:693.
- 1233 Efstathiou, G. A., Beare, R. J., Osborne, S., & Lock, A. P. (2016). Grey zone sim-  
 1234 ulations of the morning convective boundary layer development. *J. Geophys.*  
 1235 *Res. Atmos.*, *121*:9.
- 1236 Efstathiou, G. A., & Plant, R. S. (2019). A dynamic extension of the pragmatic  
 1237 blending scheme for scale-dependent sub-grid mixing. *Q. J. R. Meteorol. Soc.*,  
 1238 1–9.
- 1239 Efstathiou, G. A., Plant, R. S., & Bopape, M. M. (2018). Simulation of an evolving  
 1240 convective boundary layer using a scale-dependent dynamic smagorinsky model  
 1241 at near-gray-zone resolutions. *J. Appl. Meteorol. Clim.*, *57*, 21972214.
- 1242 Field, P. R., Brozkov, R., Chen, M., Dudhia, J., Lac, C., Hara, T., . . . McTaggart-  
 1243 Cowan, R. (2017). Exploring the convective grey zone with regional simula-  
 1244 tions of a cold air outbreak. *Q. J. R. Meteorol. Soc.*, *143*(707), 2537–2555. doi:  
 1245 10.1002/qj.3105
- 1246 Field, P. R., Cotton, R. J., McBeath, K., Lock, A. P., Webster, S., & Allan, R. P.  
 1247 (2014). Improving a convection-permitting model simulation of a cold air  
 1248 outbreak. *Q. J. R. Meteorol. Soc.*, *140*, 124–138.
- 1249 Fiori, E., Parodi, A., & Siccardi, F. (2010). Turbulence closure parameterization and  
 1250 grid spacing effects in simulated supercell storms. *J. Atmos. Sci.*, *67*(12), 3870–  
 1251 3890.
- 1252 Goger, B., Rotach, M. W., Gohm, A., Fuhrer, O., Stiperski, I., & Holtslag, A. A. M.  
 1253 (2018). The impact of three-dimensional effects on the simulation of turbulence  
 1254 kinetic energy in a major Alpine valley. *Boundary-Layer Meteorol.*, *168*(1),  
 1255 1–27.
- 1256 Green, B. W., & Zhang, F. (2015). Numerical simulations of Hurricane Katrina  
 1257 (2005) in the turbulent gray zone. *J. Adv. Model. Earth Syst.*, *7*, 142–161. doi:  
 1258 10.1002/2014MS000399
- 1259 Hagelin, S., Auger, L., Brovelli, P., & Dupont, O. (2014). Nowcasting with the  
 1260 AROME model: First results from the high-resolution AROME airport.  
 1261 *Weath. and Forecasting*, *29*, 773–787.
- 1262 Hanley, K. E., Plant, R. S., Stein, T. H. M., Hogan, R. J., Nicol, J. C., Lean, H. W.,

- 1263 ... Clark, P. A. (2014). Mixing-length controls on high-resolution simula-  
 1264 tions of convective storms. *Q. J. R. Meteorol. Soc.*, *141*(686), 272-284. doi:  
 1265 10.1002/qj.2356
- 1266 Hatlee, S. C., & Wyngaard, J. C. (2007). Improved subfilter-scale models from the  
 1267 HATS field data. *J. Atmos. Sci.*, *64*, 1694-1705.
- 1268 Honnert, R., Couvreux, F., Masson, V., & Lancz, D. (2016). Sampling of the struc-  
 1269 ture of turbulence : Implications for parameterizations at sub-kilometric scales.  
 1270 *Boundary-Layer Meteorol.*, *2:27*, doi: 10.3389/feart.2014.00027.
- 1271 Honnert, R., & Masson, V. (2014). What is the smallest physically ac-  
 1272 ceptable scale for 1d turbulence schemes? *Front. Earth Sci.*, *2:27*, doi:  
 1273 10.3389/feart.2014.00027.
- 1274 Honnert, R., Masson, V., & Couvreux, F. (2011). A diagnostic for evaluating the  
 1275 representation of turbulence in atmospheric models at the kilometric scale. *J.*  
 1276 *Atmos. Sci.*, *68*, 3112-3131.
- 1277 Hourdin, F., Couvreux, F., & Menut, L. (2002). Parameterization of the dry convec-  
 1278 tive boundary layer based on a mass flux representation of thermals. *J. Atmos*  
 1279 *Sci.*, *59*, 1105-1122.
- 1280 Huq, S., De Roo, F., Raasch, S., & Mauder, M. (2014). Vertical grid nesting for  
 1281 improved surface layer resolution in large-eddy simulation. In *21st symp. on*  
 1282 *boundary layers and turbulence*.
- 1283 Ito, J., Hayashi, S., Hashimoto, A., Ohtake, H., Uno, F., Yoshimura, H., ... Ya-  
 1284 mada, Y. (2017). Stalled improvement in a numerical weather prediction  
 1285 model as horizontal resolution increases to the sub-kilometer scale. *SOLA*, *13*,  
 1286 151-156. doi: 10.2151/sola.2017-028
- 1287 Ito, J., Niino, H., & Nakanishi, M. (2014). Horizontal turbulent diffusion in a con-  
 1288 vective mixed layer. *J. Fluid Mech.*, *758*, 553-564. doi: 10.1017/jfm.2014.545
- 1289 Ito, J., Niino, H., Nakanishi, M., & Moeng, C.-H. (2015). An extension of Mellor-  
 1290 Yamada model to the terra incognita zone for dry convective mixed layers in  
 1291 the free convection regime. *Boundary-Layer Meteorol.*, *157(1)*, 23-43.
- 1292 Kealy, J., Efstathiou, G. A., & Beare, R. J. (2019). The onset of resolved boundary-  
 1293 layer turbulence at grey-zone resolutions. *Boundary-Layer Meteorol.*, *171*, 31-  
 1294 52.
- 1295 Kelly, M., Wyngaard, J. C., & Sullivan, P. P. (2009). Application of a subfilter-scale  
 1296 flux model over the ocean using OHATS field data. *J. Atmos. Sci.*, *66(10)*,  
 1297 3217-3225.
- 1298 Khouider, B., Biello, J., & Majda, A. (2010). A stochastic multicloud model for  
 1299 tropical convection. *Commun. Math. Sci.*, *8*, 187216.
- 1300 Kitamura, Y. (2015). Estimating dependence of the turbulent length scales on model  
 1301 resolution based on a priori analysis. *J. Atmos. Sci.*, *72*, 750-762.
- 1302 Kitamura, Y. (2016). Application of the new turbulence length scale for the terra  
 1303 incognita range to numerical simulations of a convective boundary layer. *J.*  
 1304 *Metorol. Soc. Japan*, *94*, 491-506.
- 1305 Kleissl, J., Kumar, V., Meneveau, C., & Parlange, M. B. (2006). Numerical study  
 1306 of dynamic Smagorinsky models in large-eddy simulation of the atmospheric  
 1307 boundary layer: Validation in stable and unstable conditions. *Water Resources*  
 1308 *Res.*, *42*. doi: 10.1029/2005WR004685
- 1309 Kober, K., & Craig, G. C. (2016). Physically based stochastic perturbations (PSP)  
 1310 in the boundary layer to represent uncertainty in convective initiation. *J. At-*  
 1311 *mos. Sci.*, *73*, 2893-2911.
- 1312 Kuettner, J. P. (1974). General description and central program of GATE. *Bull.*  
 1313 *Amer. Meteorol. Soc.*, *55*, 712-719.
- 1314 Kurowski, M., & Teixeira, J. (2018). A scale-adaptive turbulent kinetic energy clo-  
 1315 sure for the dry convective boundary layer. *J. Atmos. Sci.*, *75(2)*, 675-690.
- 1316 Lac, C., Chaboureaud, J.-P., Masson, V., Pinty, J.-P., Tulet, P., Escobar, J., ...  
 1317 Wautelet, P. (2018). Overview of the Meso-NH model version 5.4 and its



- 1318 applications. *Geosci. Model Dev.*, *11*, 1929–1969.
- 1319 Lancz, D., Szinta, B., & Honnert, R. (2017). Modification of shallow convection  
1320 parametrization in the gray zone in a mesoscale model. *Boundary-Layer Mete-*  
1321 *orol.*
- 1322 Lappen, C.-L., & Randall, D. A. (2001). Toward a unified parameteriza-  
1323 tion of the boundary layer and moist convection. Part I: A new type of  
1324 mass-flux model. *J. Atmos. Sci.*, *58*(15), 2021–2036. Retrieved from  
1325 [https://doi.org/10.1175/1520-0469\(2001\)058<2021:TAUPOT>2.0.CO;2](https://doi.org/10.1175/1520-0469(2001)058<2021:TAUPOT>2.0.CO;2)  
1326 doi: 10.1175/1520-0469(2001)058<2021:TAUPOT>2.0.CO;2
- 1327 Lazeroms, W. M. J., Svensson, G., Bazile, E., Brethouwer, G., Wallin, S., & Jo-  
1328 hansson, A. V. (2016, Oct 01). Study of transitions in the atmospheric  
1329 boundary layer using explicit algebraic turbulence models. *Boundary-Layer*  
1330 *Meteorol.*, *161*(1), 19–47. Retrieved from [https://doi.org/10.1007/](https://doi.org/10.1007/s10546-016-0194-1)  
1331 [s10546-016-0194-1](https://doi.org/10.1007/s10546-016-0194-1) doi: 10.1007/s10546-016-0194-1
- 1332 Lean, H. W., Clark, P. A., Dixon, M., Roberts, N. M., Fitch, A., Forbes, R., & Hal-  
1333 liwell, C. (2008). Characteristics of high-resolution versions of the Met Office  
1334 Unified Model for forecasting convection over the United Kingdom. *Mon. Wea.*  
1335 *Rev.*, *136*(9), 3408–3424.
- 1336 LeMone, M. A., Chen, F., Tewari, M., Dudhia, J., Geerts, B., Miao, Q., ... Gross-  
1337 man, R. L. (2010). Simulating the IHOP\_2002 fair-weather CBL with the  
1338 WRF-ARW-Noah modeling system. Part II: Structures from a few kilome-  
1339 ters to 100 km across. *Mon. Wea. Rev.*, *138*(3), 745–764. Retrieved from  
1340 <https://doi.org/10.1175/2009MWR3004.1> doi: 10.1175/2009MWR3004.1
- 1341 Leoncini, G., Plant, R. S., Gray, S. L., & Clark, P. A. (2010). Perturbation growth  
1342 at the convective scale for CSIP IOP18. *Q. J. R. Meteorol. Soc.*, *136*, 653–670.
- 1343 Leroyer, S., Blair, S., Mailhot, J., & Strachan, I. B. (2011). Microscale nu-  
1344 merical prediction over Montreal with the Canadian external urban mod-  
1345 eling system. *J. Appl. Meteorol. Climatol.*, *50*(12), 2410–2428. doi:  
1346 10.1175/JAMC-D-11-013.1
- 1347 Lilly, D. K. (1967). The representation of small-scale turbulence in numerical sim-  
1348 ulation experiments. *Proc. IBM Scientific Computing Symp. on Environmental*  
1349 *Sciences*, 195.
- 1350 Lock, A. P., Brown, A. R., Bush, M. R., Martin, G. M., & Smith, R. N. B. (2000).  
1351 A new boundary layer mixing scheme. Part I : Scheme description and  
1352 single-column model tests. *Mon. Wea. Rev.*, *128*(9), 3187–3199. doi:  
1353 10.1175/1520-0493(2000)128<3187:ANBLMS>2.0.CO;2
- 1354 Malavelle, F. F., Haywood, J. M., Field, P. R., Hill, A. A., Abel, S. J., Lock, A. P.,  
1355 ... McBeath, K. (2014). A method to represent subgrid-scale updraft velocity  
1356 in kilometer-scale models: Implication for aerosol activation. *J. Geophys. Res.*  
1357 *Atmos.*, *119*(7), 4149–4173. doi: 10.1002/2013JD021218
- 1358 Martinet, M., Nuissier, O., Duffourg, F., Ducrocq, V., & Ricard, D. (2017). Fine-  
1359 scale numerical analysis of the sensitivity of the HyMeX IOP16a heavy pre-  
1360 cipitating event to the turbulent mixing-length parametrization. *Q. J. R.*  
1361 *Meteorol. Soc.*, *143*, 31223135. doi: 10.1002/qj.3167
- 1362 Mason, P. J., & Brown, A. R. (1999). On subgrid models and filter operations in  
1363 large eddy simulations. *J. Atmos. Sci.*, *56*, 21012104.
- 1364 Mason, P. J., & Thomson, D. J. (1992). Stochastic backscatter in large-eddy simu-  
1365 lations of boundary layers. *J. Fluid Mech.*, *242*, 5178.
- 1366 Mellor, G. L., & Yamada, T. (1982). Development of a turbulence closure model for  
1367 geophysical fluid problems. *Rev. Geophys.*, *20*(4), 851–875.
- 1368 Mirocha, J., Kirkil, G., Bou-Zeid, E., Chow, F. K., & Kosovic, B. (2013). Transition  
1369 and equilibration of neutral atmospheric boundary layer flow in one-way nested  
1370 large-eddy simulations using the weather research and forecasting model. *Mon.*  
1371 *Wea. Rev.*, *141*, 918–940.
- 1372 Muñoz-Esparza, D., Kosović, B., Mirocha, J., & van Beeck, J. (2014, Dec 01).

- 1373 Bridging the transition from mesoscale to microscale turbulence in numerical  
1374 weather prediction models. *Boundary-Layer Meteorol.*, 153(3), 409–440. doi:  
1375 10.1007/s10546-014-9956-9
- 1376 Nakanishi, M., & Nino, H. (2009). Development of an improved turbulence closure  
1377 model for the atmospheric boundary layer. *J. Meteorol. Soc. Japan*, 87(5),  
1378 895-912. doi: 10.2151/jmsj.87.895
- 1379 Neggers, R. A. J., Griewank, P. J., & Heus, T. (2019). Power-law scaling in  
1380 the internal variability of cumulus cloud size distributions due to subsam-  
1381 pling and spatial organization. *J. Atmos. Sci.*, 76(6), 1489-1503. doi:  
1382 10.1175/JAS-D-18-0194.1
- 1383 Neggers, R. A. J., Koehler, M., & Beljaars, A. A. M. (2009). A dual mass flux  
1384 framework for boundary-layer convection. Part I: Transport. *J. Atmos. Sci.*,  
1385 66, 1465-1487. doi: 10.1175/2008JAS2635.1
- 1386 Neggers, R. A. J., Siebesma, A. P., & Jonker, H. J. J. (2002). A multiparcel model  
1387 for shallow cumulus convection. *J. Atmos. Sci.*, 59, 1655-1668.
- 1388 O'Neill, J. J., Cai, X.-M., & Kinnersley, R. (2015). A generalised stochastic  
1389 backscatter model: large-eddy simulation of the neutral surface layer. *Q. J.  
1390 R. Meteorol. Soc.*, 141, 2617-2629.
- 1391 Orlanski, I. (1975). A rational subdivision of scales for atmospheric processes. *Bull.  
1392 Amer. Meteorol. Soc.*, 56, 527-530.
- 1393 Palmer, T. (2001). A nonlinear dynamical perspective on model error: A pro-  
1394 posal for non-local stochastic-dynamic parametrization in weather and climate  
1395 prediction models. *Q. J. R. Meteorol. Soc.*, 127, 279-304.
- 1396 Palmer, T. (2012). Towards the probabilistic Earth-system simulator: A vision  
1397 for the future of climate and weather prediction. *Q. J. R. Meteorol. Soc.*, 138,  
1398 841-861.
- 1399 Park, S. (2014). A Unified Convection Scheme (UNICON). Part I: Formulation. *J.  
1400 Atmos. Sci.*, 71, 3902-3930. doi: 10.1175/JAS-D-13-0233.1
- 1401 Pergaud, J., Masson, V., Malardel, S., & Couvreux, F. (2009). A parametrisation of  
1402 dry thermals and shallow cumuli for mesoscale numerical weather prediction.  
1403 *Boundary-Layer Meteorol.*, 132, 83-106.
- 1404 Petch, J. C., Brown, A. R., & Gray, M. E. B. (2002). The impact of horizontal reso-  
1405 lution on the simulations of convective development over land. *Q. J. R. Meteo-  
1406 rol. Soc.*, 128, 2031-2044,doi:10.1256/003590002320603511.
- 1407 Plant, R. S., Bengtsson, L., & Whittall, M. A. (2015). Stochastic aspects of convec-  
1408 tive parameterization. In R. S. Plant & J.-I. Yano (Eds.), *Parameterization  
1409 of atmospheric convection. Volume 2: Current issues and new theories* (pp.  
1410 135–172). World Scientific, Imperial College Press.
- 1411 Plant, R. S., & Craig, G. C. (2008). A Stochastic Parameterization for Deep Convec-  
1412 tion Based on Equilibrium Statistics. *J. Atmos. Sci.*, 65, 87-105. doi: 10.1175/  
1413 2007JAS2263.1
- 1414 Ramachandran, S., Tandon, A., & Mahadevan, A. (2013). Effect of subgrid-scale  
1415 mixing on the evolution of forced submesoscale instabilities. *Ocean Modelling*,  
1416 66, 45-63.
- 1417 Ramachandran, S., & Wyngaard, J. (2011). Subfilter-scale modelling using transport  
1418 equations: Large-eddy simulation of the moderately convective atmospheric  
1419 boundary layer. *Boundary-Layer Meteorol.*, 139, 1-35.
- 1420 Raynaud, L., & Bouttier, F. (2017). The impact of horizontal resolution and en-  
1421 semble size for convective-scale probabilistic forecasts. *Q. J. R. Meteorol. Soc.*,  
1422 143, 3037-3047.
- 1423 Redelsperger, J. L., Thorncroft, C. D., A. Diedhiou, T. L., Parker, D. J., & Polcher,  
1424 J. (2006). African monsoon multidisciplinary analysis an international research  
1425 project and field campaign. *Bull. Amer. Meteorol. Soc.*, 87(12), 1735-1746.
- 1426 Ricard, D., Lac, C., Legrand, R., Mary, A., & Riette, S. (2013). Kinetic energy spec-  
1427 tra characteristics of two convection-permitting limited-area models AROME

- 1428 and MesoNH. *Q. J. R. Meteorol. Soc.*, *139*, 1327-1341.
- 1429 Rio, C., Hourdin, F., Couvreur, F., & Jam, A. (2010). Resolved versus parametrized  
1430 boundary-layer plumes. Part II : Continuous formulations of mixing rates for  
1431 mass-flux schemes. *Boundary-Layer Meteorol.*, *135*, 469-483.
- 1432 Roberts, N. M., & Lean, H. W. (2008). Scale-selective verification of rainfall accu-  
1433 mulations from high-resolution forecasts of convective events. *Mon. Wea. Rev.*,  
1434 *136*(1), 78-97. doi: 10.1175/2007MWR2123.1
- 1435 Sakradzija, M., Seifert, A., & Dipankar, A. (2016). A stochastic scale-aware param-  
1436 eterization of shallow cumulus convection across the convective gray zone. *J.*  
1437 *Adv. Model. Earth Syst.*, *8*(2), 786–812. Retrieved from [http://dx.doi.org/](http://dx.doi.org/10.1002/2016MS000634)  
1438 [10.1002/2016MS000634](http://dx.doi.org/10.1002/2016MS000634) doi: 10.1002/2016MS000634
- 1439 Sakradzija, M., Seifert, A., & Heus, T. (2014). Fluctuations in a quasi-stationary  
1440 shallow cumulus cloud ensemble. *Nonlin. Processes Geophys. Discuss.*, *1*, 1223-  
1441 1282. doi: 10.5194/npgd-1-1223-2014
- 1442 Seity, Y., Brousseau, P., Malardelle, S., Hello, G., Bouttier, F., Lac, C., & Masson,  
1443 V. (2011). The AROME-France convective scale operational model. *Mon.*  
1444 *Wea. Rev.*, *139*, 976-991.
- 1445 Shin, H. H., & Dudhia, J. (2016). Evaluation of PBL parameterizations  
1446 in WRF at subkilometer grid spacings: Turbulence statistics in the dry  
1447 convective boundary layer. *Mon. Wea. Rev.*, *144*(3), 1161-1177. doi:  
1448 [10.1175/MWR-D-15-0208.1](http://dx.doi.org/10.1175/MWR-D-15-0208.1)
- 1449 Shin, H. H., & Hong, S. (2013). Analysis on resolved and parameterized vertical  
1450 transports in the convective boundary layers at the gray-zone resolution. *J. At-*  
1451 *mos. Sci.*, *70*, 3248-3261.
- 1452 Shin, H. H., & Hong, S. (2015). Representation of the subgrid-scale turbulent trans-  
1453 port in convective boundary layers at gray-zone resolutions. *Mon. Wea. Rev.*,  
1454 *143*, 250-271.
- 1455 Siebesma, A. P., & Cuijpers, J. W. M. (1995). Evaluation of parametric assumptions  
1456 for shallow cumulus convection. *J. Atmos. Sci.*, *52*(6), 650–666.
- 1457 Siebesma, A. P., Soares, P. M. M., & Teixeira, J. (2007). A combined eddy-  
1458 diffusivity mass-flux approach for the convective boundary layer. *J. Atmos.*  
1459 *Sci.*, *64*, 1230-1248.
- 1460 Siebesma, P., JAKOB, C., LENDERINK, G., NEGGERS, R. A. J., TEIXEIRA,  
1461 J., van MEIJGAARD, E., ... SEVERIJNS, C. (2004). Cloud representation  
1462 in general-circulation models over the northern Pacific ocean: A EUROCS  
1463 intercomparison study. *Q. J. R. Meteorol. Soc.*, *130*, 3245-3267.
- 1464 Simon, J. S., Zhou, B., Mirocha, J. D., & Chow, F. K. (2019). Explicit filter-  
1465 ing and reconstruction to reduce grid dependence in convective boundary  
1466 layer simulations using WRF-LES. *Mon. Wea. Rev.*, *147*, 1805–1821. doi:  
1467 [10.1175/MWR-D-18-0205.1](http://dx.doi.org/10.1175/MWR-D-18-0205.1)
- 1468 Skamarock, W. C. (2004). Evaluating mesoscale NWP models using kinetic energy  
1469 spectra. *Mon. Wea. Rev.*, *132*, 3019-3032.
- 1470 Smagorinsky, J. J. (1967). General circulation experiments with the primitive equa-  
1471 tions. *Mon. Wea. Rev.*, *91*(3), 99-164. doi: 10.1175/1520-0493(1963)091<0099:  
1472 GCEWTP>2.3.CO;2
- 1473 Stein, T. H. M., Hogan, R. J., Clark, P. A., Halliwell, C. E., Hanley, K. E., Lean,  
1474 H. W., ... Plant, R. S. (2015). The DYMECS project: A statistical approach  
1475 for the evaluation of convective storms in high-resolution NWP models. *Bull.*  
1476 *Amer. Meteorol. Soc.*, *96*, 939-951.
- 1477 Stirling, A. J., & Petch, J. C. (2004). The impacts of spatial variability on the devel-  
1478 opment of convection. *Q. J. R. Meteorol. Soc.*, *130*, 3189-3206.
- 1479 Stoelinga, M. T. (1996). A potential vorticity-based study on the role of diabatic  
1480 heating and friction in a numerically simulated baroclinic cyclone. *Mon. Wea.*  
1481 *Rev.*, *124*, 849-874.
- 1482 Stull, R. B. (1984). Transient turbulence theory. Part I : The concept of eddy-

- 1483 mixing across finite distances. *J. Atmos. Sci.*, *41*, 3351-3366.
- 1484 Stull, R. B. (1988). *An introduction to boundary layer meteorology*. Kluwer Academic  
1485 Publishers.
- 1486 Sullivan, P. P., Horst, T. W., Lenschow, D. H., Moeng, C.-H., & Weil, J. C. (2003).  
1487 Structure of subfilter-scale fluxes in the atmospheric surface layer with applica-  
1488 tion to large-eddy simulation modelling. *J. Fluid Mech.*, *482*, 101–139.
- 1489 Sullivan, P. P., McWilliams, J. C., & Moeng, C.-H. (1996). A grid nesting method  
1490 for large-eddy simulation of planetary boundary-layer flows. *Boundary-Layer  
1491 Meteorol.*, *80*(1-2), 167-202.
- 1492 Sullivan, P. P., & Patton, E. G. (2011). The effect of mesh resolution on convective  
1493 boundary layer statistics and structures generated by large-eddy simulation. *J.  
1494 Atmos. Sci.*, *68*(10), 2395-2415. doi: 10.1175/JAS-D-10-05010.1
- 1495 Suselj, K., Hogan, T. F., & Teixeira, J. (2014). Implementation of a stochas-  
1496 tic eddy-diffusivity/mass-flux parameterization into the Navy Global  
1497 Environmental Model. *Weath. and Forecasting*, *29*, 1374-1390. doi:  
1498 10.1175/WAF-D-14-00043.1
- 1499 Tan, Z., Kaul, C. M., Pressel, K. G., Cohen, Y., Schneider, T., & Teixeira, J. (2018).  
1500 An extended eddy-diffusivity mass-flux scheme for unified representation of  
1501 subgrid-scale turbulence and convection. *J. Adv. Model. Earth Syst.*, *10*,  
1502 770-800.
- 1503 Teixeira, J., & Cheinet, S. (2004). A simple mixing length formulation for the  
1504 eddy-diffusivity parameterization of dry convection. *Boundary-Layer Meteorol.*,  
1505 *110*(3), 435–453.
- 1506 Lafore, J., Stein, J., Asencio, N., Bougeault, P., Ducrocq, V., Duron, J., ... Vila-  
1507 Guerau de Arellano, J. (1998). The Méso-NH atmospheric simulation system.  
1508 Part I : Adiabatic formulation and control simulation. *Annales Geophysics*,  
1509 *16*, 90-109.
- 1510 Thuburn, J., Weller, H., Vallis, G. K., Beare, R. J., & Whittall, M. (2018). A  
1511 framework for convection and boundary layer parameterization derived from  
1512 conditional filtering. *J. Atmos. Sci.*, *75*(3), 965-981. Retrieved from [https://](https://doi.org/10.1175/JAS-D-17-0130.1)  
1513 [doi.org/10.1175/JAS-D-17-0130.1](https://doi.org/10.1175/JAS-D-17-0130.1) doi: 10.1175/JAS-D-17-0130.1
- 1514 Tomassini, L., Field, P. R., Honnert, R., Malardel, S., McTaggart-Cowan, R., Saitou,  
1515 K., ... Seifert, A. (2016). The grey zone cold air outbreak global model inter-  
1516 comparison : A cross evaluation using large-eddy simulations. *J. Adv. Model.  
1517 Earth Syst.*, *9*, 39-64, doi:10.1002/2016MS000822.
- 1518 Tomassini, L., Parker, D. J., Stirling, A., Bain, C., Senior, C., & Milton, S. (2017).  
1519 The interaction between moist diabatic processes and the atmospheric circula-  
1520 tion in African Easterly Wave propagation. *Q. J. R. Meteorol. Soc.*.
- 1521 Verrelle, A., Ricard, D., & Lac, C. (2015). Sensitivity of high-resolution ideal-  
1522 ized simulations of thunderstorms to horizontal resolution and turbulence  
1523 parametrization. *Q. J. R. Meteorol. Soc.*, *141*, 433–448.
- 1524 Verrelle, A., Ricard, D., & Lac, C. (2017). Evaluation and improvement of turbu-  
1525 lence parameterization inside deep convective clouds at kilometer-scale resolu-  
1526 tion. *Mon. Wea. Rev.*, *145*(10), 3947-3967. doi: 10.1175/MWR-D-16-0404.1
- 1527 Wagner, J. S., Gohm, A., & Rotach, M. W. (2014). The impact of horizontal model  
1528 grid resolution on the boundary layer structure over an idealized valley. *Mon.  
1529 Wea. Rev.*, *142*(9), 3446-3465.
- 1530 Wagner, T. M., & Graf, H.-F. (2010). An ensemble cumulus convection parameter-  
1531 ization with explicit cloud treatment. *J. Atmos. Sci.*, *67*, 3854-3869. doi: 10  
1532 .1175/2010JAS3485.1
- 1533 Warren, R. A., Kirshbaum, D. J., Plant, R. S., & Lean, H. W. (2014). A Boscawle-  
1534 type quasi-stationary convective system over the UK southwest peninsula. *Q.  
1535 J. R. Meteorol. Soc.*, *140*(678), 240-257.
- 1536 Weckwerth, T. M., Parsons, D. B., Koch, S. E., Moore, J. A., LeMone, M. A., De-  
1537 moz, B. B., ... Feltz, W. F. (2004). An overview of the International H2O

- 1538 Project (IHOP\_2002) and some preliminary highlights. *Bull. Amer. Meteor.*  
1539 *Soc.*, 85(2), 253-278. doi: 10.1175/BAMS-85-2-253
- 1540 Weinbrecht, S., & Mason, P. J. (2008). Stochastic backscatter for cloud-resolving  
1541 models. Part I: Implementation and testing in a dry convective boundary layer.  
1542 *J. Atmos. Sci.*, 65, 123-139.
- 1543 Wyngaard, J. C. (2004). Toward numerical modelling in the 'Terra Incognita'. *J.*  
1544 *Atmos. Sci.*, 61, 1816-1826.
- 1545 Xie, Z.-T., & Castro, I. P. (2008). Efficient generation of inflow conditions for large  
1546 eddy simulation of street-scale flows. *Flow Turbulence Combust.*, 81, 449-470.
- 1547 Young, G. S., Kristovich, D. A. R., Hjelmfelt, M. R., & Foster, R. C. (2002). Rolls,  
1548 streets, waves, and more: A review of quasi-two-dimensional structures in the  
1549 atmospheric boundary layer. *Bull. Amer. Meteorol. Soc.*, 83(7), 997-1002.
- 1550 Zhang, X., Bao, J.-W., Chen, B., & Grell, E. D. (2018). A three-dimensional scale-  
1551 adaptive turbulent kinetic energy scheme in the WRF-ARW model. *Mon.*  
1552 *Wea. Rev.*, 146(7), 2023-2045. doi: 10.1175/MWR-D-17-0356.1
- 1553 Zhou, B., Simon, J. S., & Chow, F. K. (2014). The convective boundary layer in the  
1554 terra incognita. *J. Atmos. Sci.*, 71(7), 2545-2563. doi: 10.1175/JAS-D-13-0356  
1555 .1
- 1556 Zhou, B., Xue, M., & Zhu, K. (2017). A grid-refinement-based approach for mod-  
1557 eling the convective boundary layer in the gray zone: A pilot study. *J. Atmos.*  
1558 *Sci.*, 74(11), 3497-3513. doi: 10.1175/JAS-D-16-0376.1
- 1559 Zhou, B., Xue, M., & Zhu, K. (2018). A grid-refinement-based approach for model-  
1560 ing the convective boundary layer in the gray zone: Algorithm implementation  
1561 and testing. *J. Atmos. Sci.*, 75(4), 1143-1161. doi: 10.1175/JAS-D-17-0346.1